JPRS L/9409

24 November 1980

USSR Report

PHYSICS AND MATHEMATICS

(FOUO 9/80)

FBIS FOREIGN BROADCAST INFORMATION SERVICE

NOTE

JPRS publications contain information primarily from foreign newspapers, periodicals and books, but also from news agency transmissions and broadcasts. Materials from foreign-language sources are translated; those from English-language sources are transcribed or reprinted, with the original phrasing and other characteristics retained.

Headlines, editorial reports, and material enclosed in brackets [] are supplied by JPRS. Processing indicators such as [Text] or [Excerpt] in the first line of each item, or following the last line of a brief, indicate how the original information was processed. Where no processing indicator is given, the information was summarized or extracted.

Unfamiliar names rendered phonetically or transliterated are enclosed in parentheses. Words or names preceded by a question mark and enclosed in parentheses were not clear in the original but have been supplied as appropriate in context. Other unattributed parenthetical notes within the body of an item originate with the source. Times within items are as given by source.

The contents of this publication in no way represent the policies, views or attitudes of the U.S. Government.

APPROVED FOR RELEASE: 2007/02/08: CIA-RDP82-00850R000300050029-2

JPRS L/9409

24 November 1980

USSR REPORT

PHYSICS AND MATHEMATICS

(FOUO 9/80)

CONTENTS

LASERS AND MASERS

UDC 621.311.6:621.373.826

LASER POWER SUPPLIES

Moscow ISTOCHNIKI PITANIYA LAZEROV in Russian 1980, signed to press 27 Sep 79 pp 2-4, 102

[Annotation, foreword and table of contents from book by Vladimir Mikhaylovich Vakulenko and Lev Pavlovich Ivanov, Izdatel'stvo Sovetskoye Radio, 10,000 copies, 102 pages]

[Text] Electrical circuits are discussed, designed to enable the operation of laser emitters in the continuous and pulsed modes. Principal attention is paid to questions relating to the design of power supplies for solid-state and gas lasers. A description is given of circuits for charging units and control systems and their functional components having improved noise immunity and precision of response, as well as of practical circuits for power supplies with an indication of features of their design and operation.

This book is intended for a wide range of specialists involved in the development and operation of lasers.

Foreword

The contemporary stage in the development of laser technology is characterized by a steady growth in the number of developments of laser units and instruments for various purposes, by the expansion of their industrial output and by their introduction in many areas of science, engineering and production. The laser has become an irreplaceable means of improving the efficiency of scientific investigations, labor productivity and the quality of products manufactured.

According to the customary definition, a laser consists of an emitter and a power supply. Depending on its purpose, the structure of a laser unit can include, in addition to the laser, an optical-mechanical unit, equipment for controlling the laser emission, equipment for measuring and stabilizing emission parameters, a cooling unit, automation equipment and the like. Each of these functional components plays an important role in ensuring a specific capacity for work of the unit.

This book is devoted to questions relating to the development of power supplies for different types of lasers for industrial purposes. Information on the design principles and key features of laser power supplies can be found in a number of studies on laser technology [1-3]. Literature is available which can be used in developing individual functional components of power supplies. But the principal information on the electrical circuits, characteristics and parameters of laser power supplies is contained in numerous domestic and foreign periodicals, is reflected in part in advertising material or is presented in accompanying technical documentation for products manufactured by industry. This fact creates not a few difficulties both for developers of these power supplies and for specialists involved in the operation of laser units.

Systematized and generalized data on laser power sources will make it possible, the authors believe, if not to utilize completely the solutions suggested, then at least to choose the direction for development. It is exactly this which is the purpose of this book. Principal attention is paid to a description of practical circuits for power supplies and for the most important individual functional components of which these supplies consist.

A description is given of the methods and circuits for firing the gas discharge units included in the structure of laser emitters. Various methods are discussed, of converting voltage sources into current sources, since the external characteristic of the latter ensures stable powering of the gas discharge and minimal power losses in the charging of the capacitive energy storage elements which are used in pulsed power supplies. Circuits and key calculation equations are presented for selecting elements of the discharge circuit of a pulsed emitter and the charging devices for capacitive energy storage elements.

Interaction of the functional components of power supplies is governed by the control system, which ensures the accuracy and stability of parameters and the output and synchronization of signals, and assigns the kind of operation for the laser emitter. Along with the general principles for the design of converting equipment, in the development of power supplies for laser emitters a number of specific requirements arise, occasioned by the distinctiveness of the volt-ampere characteristics of emitters and features of their operating modes. Of these requirements the principal ones are discussed in describing the circuits of power supplies for solid-state, gas and semiconductor lasers. The majority of the circuits presented for power supplies have passed tests under laboratory and production conditions and have earned good recommendations.

The authors thank the reviewers, candidates of technical sciences A.L. Vasserman and V.I. Pshenichnikov for their valuable comments made in preparation of the manuscript and Candidate of Technical Sciences E.A. Lukin, on whose initiative this book was written. Great assistance was rendered

to the authors in formation of the manuscript by Ye.Ya. Borodulina and L.S. Pavlova.

We request that comments and remarks on the content of this book be sent to the address of Izdatel'stvo Sovetskoye Radio, Moscow, Glavpochtamt, a/ya 693.

CONTENTS Page

[176-8831]

8831
CSO: 1862

UDC 621.378

NONLINEAR OPTICAL PHENOMENA IN ORGANIC COMPOUNDS

Kiev NELINEYNYYE OPTICHESKIYE YAVLENIYA V ORGANICHESKIKH SOYEDINENIYAKH in Russian 1979 signed to press 20 Apr 79 pp 4-6, 382-383

[Annotation, foreword and table of contents from book by Yevgeniy Aleksandrovich Tikhonov and Marat Terent'yevich Shpak, Izdatel'stvo Naukova Dumka, 1000 copies, 384 pages]

[Text] In this monograph are discussed phenomena which take place in molecular crystals and liquids when they interact with strong electromagnetic fields in the optical band. An investigation is made of the mechanisms of processes of induced emission, which are based on luminescence, Raman scattering and the generation of optical harmonics. Considerable attention is paid to the material aspect of the problem and to the practical method, associated with it, of implementing various types of frequency-tunable lasers. For total comprehension of the material in the book is included basic information on classical spectroscopy and the luminescence of organic compounds.

Intended for scientific personnel, graduate students and students specializing in quantum electronics and nonlinear spectroscopy.

Foreword

Organic compounds are of exceptionally great importance in nature and in man's practical work. Their use in photography, medicine, light industry, nuclear engineering, etc., is well known. In spite of the complexity of their structure, molecules of dyes have been the subject of numerous investigations by scientists. Indeed, an entire epoch of investigations of the photophysical properties of these compounds is associated with the names of the Soviet physicists S.I. Vavilov, V.L. Levshin and A.N. Terenin.

The development of quantum electronics has renewed interest in the study of dyes, but on a new scientific methodology and practical base. The effect of nonlinear optical absorption discovered by S.I. Vavilov in the "prelaser era" formed the basis of the operation of passive laser Q switches (1964). This successful application, which made it possible to

Increase the radiated power of solid-state lasers to several dozen megawatts, was followed logically by the experimental discovery of the effect of the generation of light in molecular solutions of dyes (1965-1966), which had been preceded by successful theoretical research, primarily by the studies of Soviet physicists headed up by B.I. Stepanov. It is interesting to emphasize in this connection that the principles, known up to that time, of selecting active media of promise for lasing did not point toward solutions of dyes, with their broad luminescence bands. Therefore, the first experiments which ultimately proved to be successful were formulated on a different theoretical basis, i.e., the detection of induced Raman resonance scattering in these systems.

The new vast range of application of dyes in quantum electronics, unlike their technological utilization, requires good knowledge of the electron vibrational structure of complex molecules and of the interaction of these systems with strong optical fields.

Under conditions of the rapid introduction of the results of scientific studies into the practical sphere, even today lasers employing dyes have been the subject of production and use on a growing scale. Dyes with the most diverse kinetic and spectral parameters are required for developers of practical systems. The problem of the purposeful creation of dyes satisfying the various requirements of practical application can be solved in the process of the accumulation of spectroscopic information when working with the systems available.

This monograph offers the required information to the investigator using a laser employing solutions of dyes with its highly diverse properties and capabilities. In this book are discussed questions relating to the classical spectroscopy of complex molecules (chap 1), which creates the basis for a discussion of nonlinear absorption, amplification, lasing and superfluorescence (chaps 2 and 3). In chap 4 are presented data on the many-photon interaction of light with molecular solutions and crystals of organic compounds (Raman scattering, generation of harmonics and many-photon absorption).

Since the subject matter of this study belongs to a swiftly developing field of knowledge, it is obvious that by the time of its publication essentially new results will have been obtained regarding the generation of light in the gas phase of complex molecules, lasers utilizing dyes with new optical pumping sources, lasers with distributed feedback, many-photon processes, etc.

The authors express their gratitude to the colleagues together with whom they arrived at an understanding of many of the questions discussed.

CONTENTS

[174-8831]

8831
CSO: 1862

UDC 539.1

OPTICAL RESONATORS AND THE PROBLEM OF THE DIVERGENCE OF LASER EMISSION

Moscow OPTICHESKIYE REZONATORY I PROBLEMA RASKHODIMOSTI LAZERNOGO IZLUCHENIYA in Russian 1979 signed to press 29 Oct 79 pp 2-5

[Annotation and table of contents from book by Yuriy Alekseyevich Anan'yev, Izdatel'stvo Nauka, 4000 copies, 328 pages]

[Text] In this book are discussed the fundamentals of the theory of optical resonators and factors governing the divergence of laser emission are discussed. Principal attention is paid to the problem of producing narrow-beam emission; information is presented on various methods of reducing angular divergence. Discussed in the greatest detail are the properties of lasers with so-called unstable resonators, and methods of calculating and optimizing them are discussed; the features of circuits used in various laser units are discussed. In this book is also presented some information on the reasons for the origin of and the nature of optical inhomogeneities in the active medium, as well as on methods making it possible to lessen the influence of these inhomogeneities.

CONTENTS

[175-8831]

8831
CSO: 1862

UDC 621.373.826

THE PROPAGATION OF LASER ABSORPTION WAVES WITH EXPOSURE TO RADIATION AT A WAVELENGTH OF 10.6 MICROMETERS

Moscow KVANTOVAYA ELEKTRONIKA in Russian Vol 7, No 6, Jun 80 pp 1236-1240
manuscript received 26 Oct 79

[Article by A.A. Bakoyev, L.I. Nikolashina and N.V. Prokopenko]

[Text] The results of an experimental study of the parameters of laser absorption waves (LVP) which propagate with exposure to radiation at a wavelength of 10.6 micrometers in a range of power densities of $q = 2$ to 10 MW/cm^2 are given. The data obtained on the developmental dynamics, the temperature, the optical properties and the pressures at the target and in the plasma are compared with calculations of LVP parameters based on the theories of light detonation and subsonic radiation waves (DRV). The conclusion is drawn on the basis of the comparison made that an LVP which propagates with the action of radiation at $\lambda = 10.6$ micrometers is a subsonic radiation wave. The existing quantitative lack of agreement between the experimental and theoretical data is explained by the existence of a mechanism which increases the gas mass capture rate, w, by the radiation wave. Nonequilibrium heating of the electrons and turbulization of the gas flow at the subsonic radiation wave front can serve as possible mechanisms for increasing w.

An increase in the rate of laser machining of a material can be achieved by boosting the radiation flux density, q, at its surface. However, with an increase in q, absorption waves appear close to the surface of the material in the ambient air, where these waves are sustained by the laser radiation, and which we shall call laser absorption waves (LVP's).

The presence of a laser absorption wave sharply reduces the processing efficiency, and for this reason, a study of the physical mechanisms of their occurrence and propagation is of practical interest for the optimization of technological processes.

It was shown in papers [1-3] that with the action of radiation at $\lambda = 10.6$ μm on opaque materials, LVP's occur at radiation fluxes of $q \sim 1$ MW/cm^2. A number of theoretical models have been proposed to describe the propagation of LVP's in a gas: light detonation (SD) [4], radiation wave [5] and "slow" combustion [4].

The data on the various aspects of infrared radiation on opaque materials have been given in the literature [1-3, 6-10]: on the propagation velocities of the LVP front, the pressure at the target, the integral spectral characteristics and the brightness temperature of the plasma flare - but these do not permit an overall comparison between experimental results and the results of calculations based on the various models. This is related to the lack of data on the equilibrium temperature and the optical properties of the LVP plasma for a single experiment. This paper is devoted to a comprehensive study of the parameters of laser absorption waves for the purpose of comparing the results obtained with existing theoretical models.

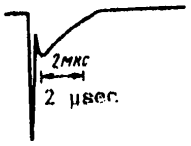

Figure 1. The lasing pulse waveform for an electrical dischrage CO_2 laser.

An electrical discharge CO_2 laser with a pulse energy of up to 50 J (Figure 1) was used in the experiments. No more than 15 to 20% of the overall energy was contained in the leading small lasing peak, and the power in it was three to five times greater than the average pulse power. The base pulse width was 2.5 to 4.0 μsec.

The laser radiation was converged by a lens having a focal distance of 100 cm onto the surface of an aluminum sample in a rectangular spot with dimensions of 1.2 x 1.2 cm. The energy distribution in a 0.8 x 0.8 cm central portion of the spot was rather homogeneous. The values of the average instantaneous radiation power density over the spot, q_t, were computed from the measurement data for the timewise course of the lasing and energy falling in a spot with a diameter of 1 cm. The average value of the radiation flux density over a lasing pulse, $\bar{q}$ was taken as equal to the ratio of the radiation energy in a 1 cm diameter spot to

its area and the pulse width. According to the estimates, the error in the determination of the values of $\bar{q}$ and q_t amounted to $\pm$ 20 percent. The quantity q was varied in the experiments in a range of 2 to 8 MW/cm^2. The velocity of the plasma flare front was determined by means of a type SFR [streak camera] photo recorder operating in a slot scanning mode with a record speed of 3.0 km/sec. The timewise tying of the photoscans to the lasing pulse was realized with a precision of $\pm$ 0.2 μsec.

The space-time distributions of the temperature in the plasma flare was measured by means of a self-illuminating circuit [11], mounted on a common axis with the SFR, which took frame by frame photographs of the flare in a spectral range of 488 $\pm$ 2 nm at a rate of 2 frames per μsec. The utilization of a mirror raster in the self-illuminating circuit made it possible to obtain in one frame of a SFR photograph with a spatial resolution of 0.1 cm information on the brightness and optical thickness of the flare in a direction perpendicular to the laser beam. The brightness temperature T_b and the equilibrium temperature T_e [based on Kirchoff's law were determined from these data, as well as the absorption coefficient of the plasma in the selected spectral range.

The recording of the radiation spectrum of the axial region of the flare was accomplished with a spatial resolution of about 0.1 cm and a time resolution of about 0.5 μsec using the procedure described in detail in [12]. Absolute values of the radiation intensity during the recording of the spectra and the self-illumination of the plasma were obtained by means of a type EV-45 calibrated light source. The timewise curve of the pressure on the surface of the target at the center of the irradiation spot was recorded by a rod piezoelectric transducer 0.3 cm in diameter with a time resolution of no worse than 0.8 μsec.

It was determined in experiments to study the dynamics of plasma flare development that when $\bar{q} \geq 2$ MW/cm^2, the laser absorption wave arises at the surface of the target no later than 0.2 μsec following the onset of the lasing pulse. Primary attention in this paper has been devoted to the study of the LVP parameters during the action of the laser pulse.

Measured values of the flare front propagation velocity v_ϕ are plotted in Figure 2 as a function of q_t, as well as the calculation results based on the light detonation theory of [4] and the subsonic radiation wave theory (DRV) of [17]. It follows from Figure 2 that, first of all, the measured values of v_ϕ are uniquely determined by q_t, and secondly, the experimental curve for v_ϕ (q_t) is positioned between the curves computed from the indicated theoretical models.

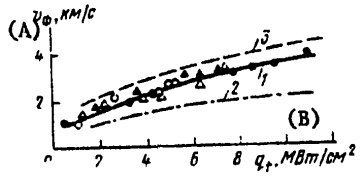

Figure 2. The flare front propagation velocity v_ϕ as a function of q_t.

Key: 1. The experimental curve;
2. Calculation based on the subsonic radiation wave model [17];
3. Calculation based on the light detonation theory [4].

The points designated with identical symbols correspond to measurements of v_ϕ during a single lasing pulse.

A. v_ϕ, km/sec;
B. q_t, MW/cm^2.

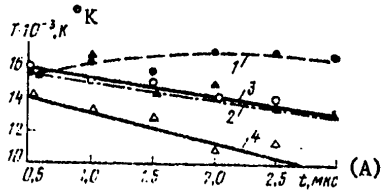

Figure 3. The timewise curve for the brightness (1, 2, 4) and equilibrium (3) temperatures of the plasma.

Key: 1. λ = 500 nm;
2. λ = 400 nm;
3,4. λ = 488 nm (self-transillumination);

A. t, microseconds.

An analysis of the time resolved spectra showed that throughout the investigated wavelength range (380--680 nm), the radiation spectrum of the flare during a lasing pulse is determined by the continuous background radiation and the radiation of the strongly widened lines of the

singly charged ions of nitrogen and oxygen. It was also established that the lines of ionized air appear no later than 0.5 μsec (the exposure time of the spectra) after the onset of lasing, while the lines of the target material are not present.

The value of T_b of the plasma immediately behind the LVP front was determined from the intensity of the groups of lines positioned in the spectral regions of 400 ± 20 nm and 500 ± 20 nm, i.e., there where the brightness temperature reached the maximum value. The results of these measurements for various points in time during the lasing pulse, as well as a comparison of them with T_e, obtained by the self-illumination method, are shown in Figure 3.

As can be seen from Figure 3, the values of T_b determined from the intensities of the lines, are in agreement within the limit of experimental error with the corresponding values of T_e obtained by the self-illumination method. The values of T_b found from measurements of the CW radiation intensity in a range of 488 ± 2 nm are (2--3) · 10^3 °K below the corresponding values of T_e, where a tendency towards an increase in the difference is observed towards the end of a lasing pulse. It should be noted that despite the substantial change in the laser radiation intensity during a lasing pulse, the value of the plasma temperature behind the LVP front changes to an insignificant extent. The data obtained in this work on the slight dependence of T_b and T_e on $\bar{q}$ are in agreement with the results of paper [5].

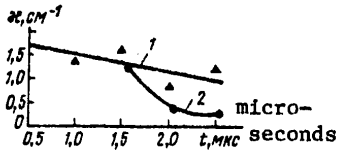

Figure 4. The coefficient of absorption for the continuous radiation behind the LVP [laser absorption wave] front (1) and in the zone between the LVP front and the target (2).

Values of the continuous absorption κ in a spectral range of 488 ± 2 nm which were found by the transillumination of the plasma flare with its own radiation in a direction perpendicular to the laser beam are shown in Figure 4. The data on κ apply to a plasma located directly behind the LVP front and to a plasma in the region between the target and the LVP front. In this region, the measured values T_e and T_b are approximately 2 · 10^3 °K lower than in the region immediately behind the LVP

front, in which case the drop in T_b with time takes place more rapidly than follows from Figure 3.

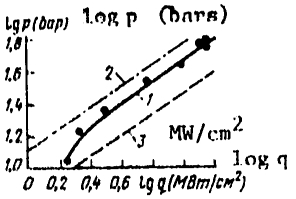

Figure 5. The curve of p_s as a function of q.

Key: 1. Experiment;
2. Calculated from the subsonic radiation wave theory of [5];
3. Calculated from the light detonation theory of [4].

By using the calculations for the optical properties of air in [13], the pressure and the absorption coefficient $\kappa_{10.6}$ at the laser radiation wavelength can be estimated from the values obtained for T and κ. It follows from the estimates made in this manner that the pressure immediately behind the front reaches a level of $p_\phi \approx 100$ bars, and in this case, the absorption coefficient amounts to $\kappa_{10.6} \approx 80$--100 cm^{-1}. The data given for T_b, T_ϕ and κ apply to $\bar{q} \approx 3$ MW/cm^2 (the maximum values of the radiation power density reached $q = 5$ MW/cm^2).

Thus, it follows from the measurement of the optical properties of the plasma flare that the liberation of laser radiation energy occurs in a narrow layer, the width of which ($l \approx 10^{-2}$ cm) is much less than the transverse dimensions of the irradiation spot ($R_0 \approx 0.5$ cm).

The measured maximum values of the pressure p_s at the surface of the target are shown in Figure 5 as a function of the maximum values of the radiation flux density. Also shown there for comparison is p_s as a function of q, computed from the subsonic radiation wave [5] and the light detonation [4] models. In the case of the calculations of p_s based on the subsonic radiation wave model, the pressure in the flare was considered to be steady-state, while to calculate the pressure at the target in the light detonation case, the following formula was used which is given in paper [14]:

$$p_s \approx p_\phi \left[\frac{(\gamma+1)}{2\gamma}\right]^{2\gamma/(\gamma-1)},$$

where γ is adiabatic exponent of the gas; p_ϕ is the pressure behind the light detonation wave front.

As can be seen from Figure 5, the measured curve for p_s as a function of q can be approximated by the expression $p_s \sim q^{2/3}$, something which is in agreement both with the light detonation model and the subsonic radiation wave model. However, the experimental curve based on the absolute value falls between the computed ones.

The width of the energy liberation zone in our experiments was much less than the size of the irradiated spot, while the height of the flare rise at the initial points in time of exposure did not exceed its diameter. This makes it possible to compare the resulting experimental data with the results of calculations based on one-dimensional models. Given in the Table are measured values of the LVP parameters, as well as their calculated values based on the light detonation and subsonic radiation wave models for $q = 5$ MW/cm^2. As can be seen from the Table, the measured values of the LVP parameters differ from those calculated based on both models.

TABLE

Parameter Параметр	Theory Теория		Эксперимент Experiment
	СД [4, 14]	ДРВ [5]	
$v_ф$, км/с km/sec	(1) 3.6	(2) 2.2	2.8
$T_ф \cdot 10^{-3}$, K °K	7.5	36	16
$p_ф$, бар	65	37	100 (оценка)
p_s, бар bars	23	37	30 (estimate)

Key: 1. Data according to the light detonation theory [4, 14];

2. Data according to the subsonic radiation wave theory [5].

The hydrodynamic mechanism for LVP propagation (light detonation) presupposes the capture of unperturbed gas by the shock wave and its subsequent heating by the laser radiation, i.e., the mass of the heated gas is completely determined by the velocity of the shock wave, which matches the velocity of the luminescent front, and the density of the gas through which it propagates. For this reason, such a great difference in the computed and measured values of the plasma temperature in an LVP makes it possible to assert that the light detonation mode is not realized in our experiments.

A shock wave which propagates opposite to the laser radiation is also generated in the subsonic radiation wave mode. The luminescent LVP

front, in accordance with this model, propagates through a shock compressible gas, but one which is transparent to laser radiation. In this case, the propagation velocity of the laser wave is somewhat less than the shock wave velocity, while the capture of the heated gas mass is determined by the radiation transfer from the LVP plasma. The lack of agreement between the measured and computed values of the temperature based on the subsonic radiation wave theory is explained, in our opinion, by the fact that there exist other mechanisms along with the radiation mechanism for LVP propagation which are capable of increasing the capture of the heated gas mass, and consequently, capable of reducing the plasma temperature behind the LVP. It should be noted that for the measured values of T, the velocity of sound in the plasma does not exceed the LVP front velocity by much, i.e., the hypothesis concerning the steady-state nature of the pressure in the plasma may not be observed.

It is proposed in paper [15] that vortex formation in the gas flow at the LVP front be treated as one of the possible mechanisms for the increase in the capture rate of the gas mass, w.

Another possible mechanism for increasing w can be nonequilibrium heating of the electrons in the electromagnetic wave field ahead of the subsonic radiation wave front. In accordance with [16], the separation of the electron temperature T_{el} from the heavy particle temperature T_a in the optical frequency range of the electromagnetic field increases with an increase in the quantum energy. It is possible that this explains the enormously better agreement between the calculations based on the subsonic radiation wave theory of [17] and the experimental data of [15], obtained for radiation at a wavelength of 1.06 μm.

We will note that plasma nonequilibrium can be substantial only ahead of the radiation wave front. According to estimates, at the end of the energy liberation region, starting with which the measurements of the parameters were made, the plasma reaches a state of local thermodynamic equilibrium.

Based on the experimental studies which have been performed and the analysis of the results obtained, the conclusion can be drawn that to describe a subsonic radiation wave propagating with the action of laser radiation at $\lambda = 10.6$ μm in a range of $q = (1\text{--}10)$ MW/cm^2, one should draw on the mechanism of additional gas mass capture besides the transfer of continuous spectrum radiation.

The authors are grateful to R.Ye. Rovinskiy for his consulation and making it possible to perform the experiments with a CO_2 laser, as

well as to A.P. Sobolev and T.V. Nenchinov for the useful discussion of the results obtained.

BIBLIOGRAPHY

1. A.N. Pirri, R.S. Schlier, D. Nortam, APPL. PHYS. LETTS., 21, 79, (1972).

2. A.I. Barchukov, F.V. Bunkin, V.I. Konov, A.M. Prokhorov, PIS'MA V ZHETF [LETTERS TO THE JOURNAL OF EXPERIMENTAL AND THEORETICAL PHYSICS], 17, 413, (1973).

3. A.A. Bakeyev, L.A. Vasil'yev, L.I. Nikolashina, N.V. Porkopenko, A.S. Churilov, V.I. Yakovlev, KVANTOVAYA ELEKTRONIKA [QUANTUM ELECTRONICS], 2, 1278, (1975).

4. Yu.P. Rayzer, "Lazernaya iskra i rasprostraneniye razryadov" ["Laser Sparking and the Propagation of Discharges"], Moscow, Nauka Publishers, 1974.

5. Ye.A. Kozik, T.V. Loseva, I.V. Nemchinov, V.V. Novikova, KVANTOVAYA ELEKTRONIKA, 5, 2,138, (1978).

6. V.P. Ageyev, A.I. Barchukov, F.V. Bunkin, V.I. Konov, KVANTOVAYA ELEKTRONIKA, 6, 78, (1979).

7. V.A. Boyko, V.A. Danilychev, V.D. Zvorykin, I.V. Kholin, A.Yu. Chugunov, PIS'MA V ZHTF [JOURNAL OF TECHNICAL PHYSICS], 2, 743, (1976).

8. V.S. Golubev, L.I. Kiselevskiy, V.N. Snopko, ZHPS [JOURNAL OF APPLIED SPECTROSCOPY], 26, 983 (1977).

9. L.R. Hettche, J.T. Schriempf, R.L. Stegman, J. APPL. PHYS., 44, 4079 (1973).

10. J.E. Lowder, D.E. Lencioni, F.W. Hilton, P.J.Hull, J. APPL. PHYS., 44, 2,579, (1973).

11. V.K. Goncharov, L.Ya. Min'ko, Ye.S. Tyunina, A.N. Chumakov, KVANTOVAYA ELEKTRONIKA, No 1 (13), 56, (1973).

12. A.A. Bakeyev, L.A. Vasil'yev, L.I. Nikolashina, N.V. Prokopenko, ZHPS, 31, 592, (1979).

13. I.V. Avilova, L.M. Biberman, V.S. Vorob'yev, V.M. Zamalin, G.A. Kobzev, A.N. Lagar'kov, A.Kh. Mnatsakyan, G.E. Norman, "Opticheskiye svoystva goryachego vozdukha" ["The Optical Properties of Hot Air"], Moscow, Nauka Publishers, 1970.

14. A.N. Pirri, PHYS. FLUIDS, 16, 1,435, (1973).

15. Ye.A. Berchenko, A.P. Sobolev, B.T. Fedyushin, KVANTOVAYA ELEKTRONIKA, 6, 1,546 (1979).

16. V.L. Ginzburg, "Rasprostraneniye elektromagnitnykh voln v plazme" ["Electromagnetic Wave Propagation in a Plasma"], Moscow, Nauka Publishers, 1967.

17. V.T. Bergel'son, T.V. Loseva, I.V. Nemchinov, PMTF [APPLIED MECHANICS AND ENGINEERING PHYSICS], 4, 22, (1974).

[173-8225]

8225
CSO: 1862

UDC 621.373.826.038.823

CHARACTERISTICS OF THE LASER RADIATION OF A PULSED PERIODIC CO_2 LASER WITH A CLOSED GAS CYCLE

Moscow KVANTOVAYA ELEKTRONIKA in Russian Vol 7, No 6, Jun 80 pp 1186-1190 manuscript received 20 Aug 79

[Article by A.A. Vedenov, S.V. Drobyazko and M.M. Korzinkin, Institute of Atomic Energy imeni I.V. Kurchatov, Moscow]

[Text] The characteristics of the laser emission of a pulsed periodic CO_2 low pressure laser with a closed gas cycle and an average power of 1 KW are given. It is experimentally demonstrated that it is possible to increase the laser pulse width by shifting the axis of the resonator down stream relative to the flow with respect to the axis of the discharge in the case of a subsonic flow of the gas mixture. A laser pulse width of 300 microseconds is obtained with a current pulse width of 1.5 microseconds.

The application of pulse periodic CO_2 lasers (CO_2 IPL) to the dimensional machining of various materials has proved to be of little effectiveness because of the occurrence of a dense plasma ahead of the target [1, 2], which absorbs a significant portion of the laser pulse energy. One of the ways of eliminating this phenomenon is increasing the laser pulse width while maintaining its overall energy and reducing the percentage of the energy in the leading edge of the power pulse, in the "little peak". This is achieved by reducing the percentage of the CO_2, increasing the precentage of N_2 in the mixture and improving the Q of the resonator [3-5]. A similar result was obtained in paper [6] by replacing the N_2 molecules with CO, the rate of transfer of the excitation from which to the upper lasing level of CO_2 is an order of magnitude lower than for nitrogen. A maximum laser pulse width of τ_p = 150 μsec with an excitation pulse width of approximately 1 μsec was obtained in

papers [3, 6] with a stable resonator where the reflection factor of the output mirror was 95 to 98 percent. When working with such a resonator in the pulsed periodic mode, the thermal loading of the mirrors becomes too great.

Another possible way of increasing the laser pulse width is shifting the axis of the resonator downstream with respect to the flow and with respect to the axis of the discharge. This method was used in an IPL with a supersonic gas mixture flow and made it possible to achieve emission pulses with a width of up to 43 μsec [7].

The characteristics of the laser emission of a low-pressure IPL with a closed gas cycle are given in this paper, and the possibility of substantially increasing the laser pulse width by means of shifting the axis of the resonator downstream beyond the discharge region with a subsonic gaseous mixture flow is experimentally demonstrated.

The experiments were performed on a CO_2 periodic pulsed laser with a closed gas cycle. The working mixture was pumped through in a direction perpendicular to the electrical field of the discharge and the optical axis by means of two 2 DVN-1500 pumps with a volumetric rate of flow of 1,500 l/sec each. The total volume of the gas circuit amounts to 2 m^3 and the leakage infiltration is no more than 0.1 mm Hg/hr, something which makes it possible to perform service life tests on the laser. An electrode system with a plasma cathode and ultraviolet preionization, described in paper [5], was used to produce the pulsed glow discharge in a volume of 4 x 4 x 50 cm. The resonator consisted of an enclosed mirror 60 mm in diameter with a radius of curvature of 10 m coated with gold and a flat germanium plate with a dielectric coating and having a reflection factor of 85 percent. The radiation flux onto the reflectors was limited by a square diaphragm 4 cm on a side. The measurement of the current J and the voltage U across the discharge gap, the energy E and the lasing pulse waveform as well as the determination of the specific energy input W and the ratio E/p for the discharge (E is the electrical field intensity and p is the pressure of the working mixture) were accomplished using the procedures described in papers [5, 8]. To measure the small signal gain k, a circuit was used which is similar to that described in paper [9], which makes it possible to record the level of the amplified and unamplified signals with a single oscilloscope (Figure 1).

The measured values for the maximum small signal gain k_{max} over a pulse as a function of the CO_2 content in the mixture (N_2:He = 1:1) with constant specific energy input of W = 300 J/(l · atm) and p = 80 mm Hg (curve 1) and as a function of the voltage across the storage capacitor, $U_п$, for a mixture of CO_2:N_2:He = 10:45:45 (curve 2) are shown in

Figure 2. Also shown in it is the specific energy input into the discharge W, as a function of the voltage across the storage capacitor when C_H = 0.2 microfarads and p = 80 mm Hg (curve 3). The curve for k_{max} as a function of the specific energy input (curve 2) is in qualitative agreement with that obtained in paper [10]. The deviation from the linear rise in k_{max} in paper [10] begins at an energy input of 0.085 eV per molecule of the CO_2 + N_2 mixture, while saturation begins at 0.2 eV for a mixture of CO_2:N_2:He = 3:10:87 with a total pressure of 100 mm Hg. In our experiments for a mixture of CO_2:N_2:He = 10:45:45 at p = 80 mm Hg, the deviation from a linear rise in k_{max} and the saturation have an onset at energy inputs of 0.07 and 0.18 eV respectively.

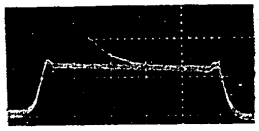

Figure 1. Typical oscilloscope trace of signals before and after amplification.

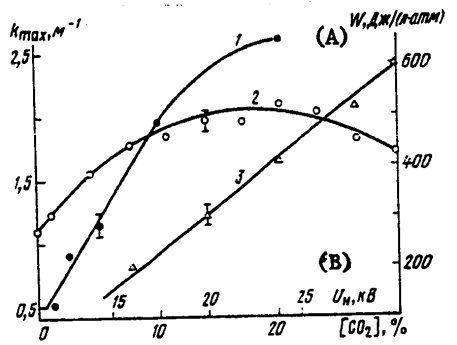

Figure 2. The curves for k_{max} (1, 2) and the specific energy input (3) as a function of the composition of the mixture (1) and the voltage across the storage capacitance (2, 3).

Key: A. W, J/(l · atm);
B. U_H [capacitor voltage], KV.

The laser pulse width is shown in Figure 3 as a function of CO_2 content in the mixture for specific energy inputs of 300 J/(l · atm) and various

positions of the resonator axis with respect to the discharge axis. The increase in the lasing pulse width in the presence of the gas flow and with the resonator offset (curves 4 and 3) is explained by the fact that when the pump-through is actuated, all of the excited gas passes through the resonator region, while without pump-through, only half of the excited gas is in the resonator region. With a drop in the overall pressure down to 40 mm Hg (curve 4), the laser pulse width increases because of the drop in the rate of collision relaxation of the upper lasing level. To explain the impact of the resonator position on the laser pulse width in the absence of pump-through (curves 1 and 2), we shall consider the processes in the stimulated portion of the gas following the completion of the discharge. The energy expended for ionization, the stimulation of the electron levels as well as for the excitation of symmetrical and deformational vibrations of the CO_2 molecules changes to thermal energy more rapidly or during the relaxation time for the 01'0 level of the deformation mode of CO_2, since intramodal exchange and exchange between symmetrical and deformational modes as well as recombination and extinguishing of electron stimulated states occurs more rapidly than does the relaxation of the 01'0 level. For our mixtures, when p = = 80 mm Hg, the relaxation time of the 01'0 level amounts to 6 to 9 μsec. The fraction of this energy from that put into the discharge depends on E/p [11] and based on estimates amounts to 50 percent in our case.

Gas heating leads to the occurrence of gas dynamic separation at the boundary with the cold gas, which decays into a shock wave and a rarefaction wave [12, 13]. The latter, in propagating through the heated gas, leads to an expansion of the heated plug and a reduction in the gas temperature and particle density in it. The characteristic half-life for k along the discharge axis is 1.5 to 2 times less than at the edge of the discharge. This is related to the greater density of the particles and temperature in the center of the discharge at the starting point in time, since at the edge of the discharge, the density and temperature of the gas begin to fall off immediately following the relaxation of the 01'0 level, i.e., after 6 to 9 μsec in our case. When the axis of the resonator coincides with the discharge axis (curve 1), the bulk of the excited gas in the lasing region is at a pressure of 80 mm Hg and the maximum temperature for the first 50 to 80 μsec, something which leads to the fast relaxation of the upper lasing level. For a resonator, the axis of which coincides with the edge of the discharge (curve 2), as soon as after 20 to 30 μsec, most of the resonator volume proves to be filled with the active medium at a reduced gas pressure and temperature, something which reduces the relaxation rate of the upper lasing level, and consequently increases the laser pulse width. We will note that when the resonator is shifted downstream relative to the flow, there is more efficient relieving of the inversion from that portion of the excited gas which expands downstream relative to the flow. Thus, only for the case of operation with short laser pulses ($\tau_p \leq 10$ μsec) can the gas be considered

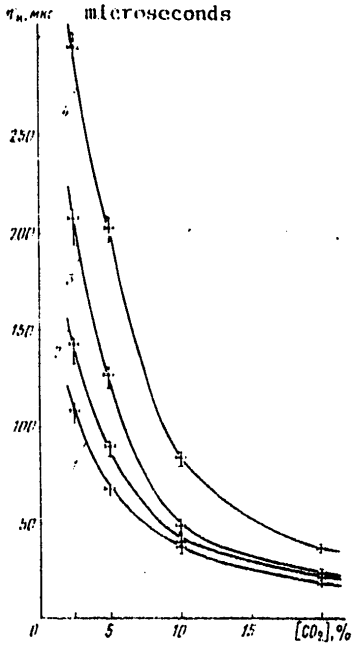

Figure 3. The laser pulse width as a function of the CO_2 content in the mixture (N_2:He = 1:1) for a resonator, the axis of which coincides with the dishcarge axis (1) or is shifted from it downstream by 2 cm (2-4).

Key: v_r = 0 (1, 2) and 80 m/sec (3, 4); p = 80 (1-3) and 40 mm Hg (4).

stationary; for the case of operation with long laser pulses ($\tau_p \gtrsim 50$ μsec), it is necessary to take into account both the expansion of the heated plug and the displacement of the gas as a result of the pump-through.

The laser pulse energy as a function of the mixture composition without gas flow-through where the resonator axis coincides with that of the discharge is shown in Figure 4 for pressures of 80 and 40 mm Hg. It can be seen that the laser pulse energy falls off with a reduction in the percentage of CO_2 in the mixture and at 1.25 percent CO_2, is 30 to 50 percent of the maximum value. We will note that in the literature [3, 6] with a pulse width of 150 μsec, the energy in a pulse amounted to only 10 to 14 percent of that obtained with an optimal mixture, something which is apparently related to the greater rate of depletion of the upper lasing level with a total working mixture pressure of p = 760 mm Hg. The optimum CO_2 concentration in terms of the laser pulse energy amounts to 20 percent in our experiments, however, in this case 20 percent of the pulse energy is concentrated in the small power peak, which when the radiation is focused causes optical flashover in front of the target which impedes its machining.

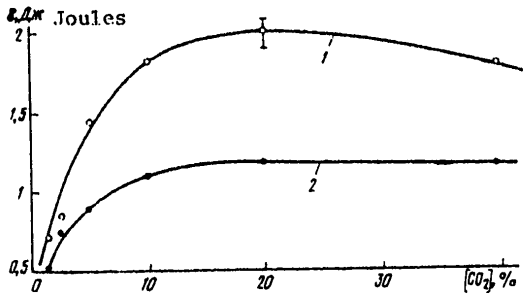

Figure 4. The laser pulse energy as a function of the CO_2 content in a mixture of (N_2:He = 1:1) for p = 80 (1) and 40 mm Hg (2); W = 300 (1) and 330 J/(1 · atm) (2).

TABLE

The Value of k and the Duration of the Existence of Amplification of τ_y at a Distance of 2 cm from the Discharge Axis Downstream with Respect to the Flow (v_{gas} = 80 m/sec).

	p = 80 мм рт. ст. p = 80 mm Hg						
U_0, кВ KV	(1) W, Дж/(1 атм)	10% CO_2		5% CO_2		2,5% CO_2	
		k, м$^{-1}$	τ_y, мкс (2)	k, м$^{-1}$	τ_y, мкс (2)	k, м$^{-1}$	τ_y, мкс (2)
16	200	1,2	415	1,0	550	1	650
20	300	1,4	340	1,2	570	1,1	650
24	440	1,5	220	1,3	430	1,25	680
28	520	1,5	190	1,2	950	1,4	670
	p = 40 мм рт. ст. p = 40 mm Hg						
16	330	1,4	580	1,6	700	0,9	650
20	520	1,5	520	1,7	700	1	700
24	700	1,7	420	1,8	760	1	720
28	930	1,6	260	1,8	800	1	800

Key: 1. W, J/(1 · atm);
2. τ_y, μsec.

Figure 5. Oscilloscope trace of the current (above) and the laser pulse (below).

Horizontal sweep is 10 μsec/div; p = 80 mm Hg; U_H = 28 KV; C_H = 0.2 microfarads; the mixture is CO_2:N_2:He = 5:47.5:47.5.

With an increase in the pressure of the working mixture, the laser pulse energy, as is well known, increases proportionally to the pressure, while its pulse width falls off in inverse proportion to the pressure. Since E/p in our experiments changes only slightly with pressure, the energy distribution in a pulse between the little peak and the wide portion of the pulse does not depend on the pressure. Thus, with an increase in the pressure of the working mixture, the power at the target averaged over the pulse increases as the sqaure of the pressure. For this reason, pulse periodic lasers with a low working mixture pressure ($p \leq 100$ mm Hg) are preferable to obtain efficient interaction with the target.

An analysis of the timewise dependence of the gain at the edge of the discharge on the pressure, the composition of the mixture and the specific energy input (see the Table) shows that with an increase in the dimensions of the active medium along the resonator axis by a factor of two to three, the lasing pulse width can be increased up to 500 to 600 μsec.

The laser radiation characteristics given in this paper were recorded, as a rule, in the single pulse mode. A pulse repetition rate of up to 500 Hz when the working mixture is pumped through during operation has no influence on the specific energy input, the laser pulse parameters or the gain. A typical waveform of the laser pulse is shown in Figure 5.

With a volumetric rate of flow of 1.5 m^3/sec and a pressure of 120 mm Hg for a mixture of CO_2:N_2:He = 10:45:45, an average power of 1 KW was obtained for an overall efficiency of 5 percent and a service life of 40 minutes (e = 2J, f = 500 Hz).

Thus, the possibility of increasing the lasing pulse width of a CO_2 laser by means of shifting the axis of the resonator downstream relative to the flow from the axis of the discharge with a subsonic flow of the gas mixture has been experimentally demonstrated. The resulting laser

pulse width of 300 μsec for a current pulse width of 1.5 μsec is a new record. We will note that to obtain laser pulses longer than 100 μsec with a reflection factor of the output mirror of 85 percent, it is necessary to operate at low pressures of the working mixture (≤ 100 mm Hg).

In conclusion, the authors would like to express their gratitude to A.G. Borkin and A.A. Nekrasov for assisting in the performance of the measurements.

BIBLIOGRAPHY

1. R.L. Stegman, J.T. Schriempf, R.L. Hettche, J. APPL. PHYS., 44, 3,675, (1973).

2. W.E. Maher, R.B. Hall, R.R. Johnson, J. APPL. PHYS., 45, 2,138, (1974).

3. A. Girard, A.S. Beaulier, IEEE J., QE-10, 521, (1974).

4. D.C. Hamilton, D.S. Sames, S.A. Ramsden, J. PHYS. E., 8, 849, (1975).

5. S.V. Drobyazko, L.G. Zhuravskiy, KVANTOVAYA ELEKTRONIKA, 6, 49, (1979).

6. D.C. Hamilton, OPTICS COMMS., 19, 339, (1976).

7. V.Yu. Baranov, D.D. Malyuta, V.S. Mezhevov, A.P. Napartovich, KVANTOVAYA ELEKTRONIKA, 3, 649, (1976).

8. A.A. Vedenov, S.V. Drobyazko, A.A. Yegorov, L.G. Zhuravskiy, V.B. Turundayevskiy, KVANTOVAYA ELEKTRONIKA, 3, 2,480, (1976).

9. R.R. Jacobs, REV. SCI. INSTR., 44, 1,146, (1973).

10. E.A. Ballik, B.K. Garside, J. Reid, T. Tricker, J. APPL. PHYS., 46, 1,323, (1975).

11. J.J. Lowke, A. Phelps, B.W. Irwin, J. APPL. PHYS., 44, 4,664, (1973).

12. G.S. Dzakowic, S.A. Wutzke, J. APPL. PHYS., 44, 5,061, (1973).

13. A.A. Vedenov, S.V. Drobyazko, V.N. Knizhnikov, V.B. Turundayevskiy, TVT [not further defined], 13, 425, (1975)

[173-8225]

8225
CSO: 1862

UDC 621.373.826.038.823

THE INFLUENCE OF THE ACTIVE MEDIUM CHARACTERISTICS ON THE OUTPUT POWER OF AN ELECTRICAL IONIZATION CO_2 LASER

Moscow KVANTOVAYA ELEKTRONIKA in Russian Vol 7, No 6, Jun 80 pp 1199-1202 manuscript received 5 Sep 79

[Article by V.Ye. Alekseyev, V.N. Grigor'yev, N.S. Klimov, A.S. Myasnikov, A.V. Olenin and V.P. Tokarev, All-Union Electrical Engineering Institute imeni V.I. Lenin, Moscow]

[Text] Experimental studies were made of the influence of the composition and velocity of the gas mixture and the position of the resonator on the output power of a CW electrical ionization CO_2 laser. Optimum relationships are found for the components of the gas mixture and the resonator position. A qualitative theoretical explanation is given for the results obtained.

Considerable progress has been made at the present time in the design of fast flow CO_2 lasers, which operate both in CW and pulse periodic modes. The output power of such lasers depends substantially on the parameters of the active pump-through medium.

Despite the importance of this question, there are no publications at the present time in which this influence is studied sufficiently completely and systematically. The influence of the mixture composition on some of the characteristics of the radiation pulse was studied in paper [1] for a single pulse mode. In paper [2], a composition of $CO_2:N_2 = 1:1$ or 1:2 is called optimal for the pulsed mode. The optimum concentration of CO_2 amounted to six percent in the CW mode in [3] for an electrical discharge laser with a helium free mixture of air and CO_2, while the figure was three to four percent in [4] for similar conditions.

The experimentally obtained functions of the output power in the CW mode of an electrical ionization CO_2 laser as a function of the composition and pump-through velocity of the gas mixture are given in this paper; the optimum position of the resonator axis relative to the pumping region is determined.

The Experimental Set-Up

The dimensions of the active pumping region of the working mixture were: length 80 cm, height 3.2 cm and the width of the dishcarge region was determined by the width of the electron beam exiting the electron gun and was equal to 5 cm. The discharge cavity of the pumping region was formed by a cathode which took the form of a copper rectangular plate cooled around the perimeter having holes 3 mm in diameter and spaced 4 mm apart. The foil assembly of the electron gun was installed above the cathode (Figure 1). The high energy electrons (150 KeV), in passing through the aluminum foil and through the holes in the cathode enter the pumping region and ionize the gaseous mixture, making it conductive. The anode consisted of 10 plates insulated from each other having dimensions of 16 x 4 cm, and arranged in two rows underneath the cathode. Each of the plates was connected through a 250 ohm resistor to the positive terminal of the power supply.

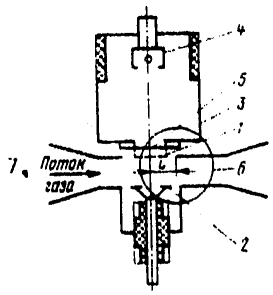

Figure 1. Schematic of the discharge chamber.

Key: 1. Cathode;
2. Anode;
3. Housing for the electron gun;
4. Cathode assembly of the electron gun;
5. Foil assembly of the electron gun;
6. Resonator;
7. Gas flow;

L is the displacement of the resonator axis downstream in the gas flow relative to the anode axis.

An open type gas dynamic channel consisted of gas tank ramps for nitrogen, helium and carbon dioxide gas, with 10 tanks each per ramp. The

gas was fed from each ramp through a reducer and cutoff valve to the mixing chamber. Each gas passed through a critical section at the input to the mixing chamber, the size of which was determined with an accuracy of 10 percent of by means of calibration blow-throughs. By changing the gas pressure ahead of the critical section in a range of 1 to 30 atm, it was possible to change the composition and velocity of the gas mixture in a wide range. The pressure was regulated in the discharge chamber (RK) by means of a variable cross-section diaphragm, installed after the discharge chamber at the input to the ballast tank having a volume of 128 m^3, and in the majority of the experiments was about 85 mm Hg, something which was determined both by the gas dynamic capabilities of the set-up and by the electron current density, limited in the steady-state mode by the strength of the foil window. Measurements of the discharge current and voltage as well as the operational time were made using an N-15 oscilloscope. The same oscilloscope was used to measure the current distribution over the sections of the anode. The voltage pulsations in the discharge did not exceed 5 percent and the current pulsations did not exceed 2 percent.

A stable resonator consisting of two spherical mirrors, the radius of curvature of which was 8 m with a diameter of 90 or 60 mm and a beam hole of 16 or 10 mm respectively was used in the experiment performed here. The radiation energy was measured by means of a calorimeter, which took the form of a massive aluminum cone with a vertex angle of 20° which was thermally insulated from the environment. The temperature difference between the cone and a specially thermally insulated metal plate was measured with a chromel-copel thermocouple, the e.m.f. of which was measured with a type F-116 microvoltmeter. The radiation was brought out into the atmosphere through a NaCl window.

The Experimental Procedure and Conditions

The ballast volume and the discharge chamber were pumped out with an RVN-2's pump down to a pressure of about 30 mm Hg prior to the start of the experiments. The variable section diaphragm was installed in a position corresponding to a specified mass rate of flow, velocity and pressure of the gas mixture into the dishcarge chamber. The level of the electron current in the discharge chamber was monitored by measuring it with a milliameter which was inserted in the circuit temporarily to ground the anode. The electron current density in the anode plane of the discharge chamber was about 10 $\mu A/cm^2$ in the majority of the experiments. When the specified level of this current was reached, the anode was disconnected from "ground" and all three cut-off valves were opened. After the specified pressure in the discharge chamber was established (something which was determined from the readings of pointer type sample manometers), the discharge voltage was applied to the anode. The

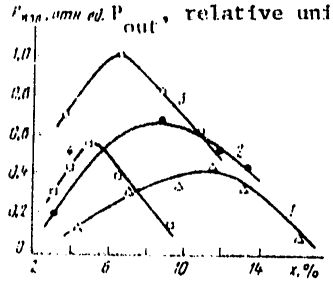

Figure 2. The relative radiation output power as a function of the percentage of CO_2 where P_{He}/P_{N_2} = = 0.5 when L = 0 (1), 2 (2), 4 (3) and 6 cm (4).

duration of the discharge was determined from an oscilloscope trace of the current. The characteristics for a semi-self maintained glow discharge, which were obtained in this work, do not fundamentally differ from similar characteristics for pressure on the order of atmospheric pressure [5] or below atmospheric [6].

The radiation power was computed as the ratio of the energy measured by the calorimeter to the time of current flow. The greatest radiation power obtained with this setup was 6.2 KW at an efficiency of 10 percent. The velocity of the gas mixture in this case was about 150 m/sec and a multipass four-mirror resonator was set up , since the length of the active region was considerably greater than the size of one reflector. The ratio of the electrical field intensity to the pressure was E/p ≈ ≈ 4.5 volt/(cm · mm Hg). For the purpose of limiting the mass rate of flow of the mixture of gases, the majority of the experiments were done at a considerably lower mixture velocity, and consequently, at a lower pumping power.

The Results of the Experiments and a Discussion of Them

The results of measurements of the output power are shown in Figure 2 as a function of the relative partial CO_2 pressure in the mixture, x = = p_{CO_2}/p_{N_2} for a constant ratio of p_{He}/p_{N_2} = 0.5. The number on each curve corresponds to the different positions of the resonator axis relative to the anode axis. The output power is referenced to the maximum value, obtained in these experiments, which is equal to 0.7 KW. For all curves, the power put into the dishcarge was 15 KW. The diameter of the spherical mirrors of the resonator was 9 cm with a beam hole of 1.6 cm, and the radius of curvature was 8 m. The velocity of the gas mixture was maintained constant within a precision of 10 percent and amounted to about 85 m/sec at a static pressure of 83 mm Hg. The difference in the potentials across the discharge for all curves was constant and equal to 1.2 KV. The heating of the mixture in the discharge was slight and amounted to $\Delta T < 50$ °K.

As follows from Figure 2, an optimal ratio of x, for which the radiation power is maximum, corresponds to each resonator position. In this case, the size of this maximum likewise passes through a maximum in step with the displacement of the resonator axis downstream relative to the flow. The course of the curves in Figure 2 can be qualitatively explained by means of the concept of a threshold length, l_π, i.e., a length over which the threshold value of the CO_2 concentration rises at the upper lasing level. This length can be found as the product of the velocity of mixture blow-through times the delay time τ of the radiation pulse, which is obtained in pulsed experiments. The value of τ was computed in [7] in a two-level approximation. Using this expression for l_π, one can derive the following relationship:

$$l_\pi = \tau_2 v_0 (1+x) \ln |1-(C\Sigma p_i A_{ci}/\tau_2 W\eta)|^{-1}, \quad (1)$$

where τ_2 is the relaxation time of the 00^01 level; v_0 is the velocity of the gas mixture in the pumping region; A_{ci} is the effective frequency of laser line widening, referenced to the widening frequency in the gas itself (CO_2); W is the specific pumping power; η is a coefficient which takes into account the fraction of the specific power expended on excitation of the upper lasing level; C is a coefficient which does not depend on the composition of the mixture or the energy input. As is well known [8], η falls off when E/p = const., with an increase in p_{CO_2}, while $\Sigma p_i A_{ci}$ increases. In our case, the second term under the logarithm sign is much less than unity, and for this reason, l_π has a minimum for a fixed position of the resonator when p_{CO_2} changes. And this means, that with a limited resonator width, the output power will have a maximum, something which is also observed in the experiments.

The existence of optimum position of the resonator (a position in which the output power has a maximum) can also be explained by the presence of a threshold length, its dependence on the velocity of the mixture (1) and the limited width of the resonator. When the axes of the resonator and the pumping region coincide, because of the large values of l_π (commensurate with the resonator width), only a portion of the resonator operates, something which leads to a reduction in output power. When the resonator axis is shifted downstream relative to the flow, the value of l_π in the resonator region falls off, since the rise in the concentration at the upper lasing level does not begin ahead of the resonator region (similar to a Q switched resonator in the pulsed mode). The area of the working portion of the resonator increases in this case, something which leads to a rise in the output power. With a further shifting of the resonator, the output power again falls off, since an ever increasing fraction of the mixture relaxes ahead of the resonator region.

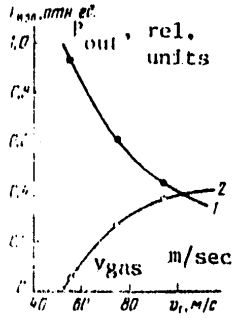

Figure 3. The relative output power in each of the two resonators with parallel axes as a function of the velocity of the mixture.

L = 0.7 cm (1) and 9 cm (2).

In our case, the diameter of the resonator mirrors is approximately twice as large as the width of the pumping region. An output power maximum, as follows from Figure 3, is obtained when the leading edge of the mirrors coincide with the axis of the pumping region at a mixture velocity of v_0 = 85 m/sec. With a different velocity of the mixture, the optimum position of the resonator will change. The dependence of the output power on the velocity was studied in an experiment with two resonators, formed by two pairs of 60 mm in diameter mirrors having beam holes of 10 mm. The axes of the resonators were set parallel at different distances from the axis of the pumping region. The axis of the first resonator was shifted downstream relative to the flow by 7 mm and the other was shifted by 90 mm. The relative output power as a function of the gas mixture velocity is shown in Figure 3 (the pumping power was 16 KW and the mixture composition was CO_2:N_2:He = 1:14:7). The course of the curves in Figure 3 confirms the influence of l_π through the mixture velocity on the laser efficiency.

Thus, it has been experimentally demonstrated that in the case of a limited width of the mirrors of the resonator, the output power of an electrical ionization CO_2 laser operating in the CW mode, depends substantially on the relationship of the partial pressures of the carbon dioxide gas and nitrogen, the velocity of the gas mixture and the position of the resonator relative to the axis of the pumping region.

It should be noted in conclusion that a reduction in l_π is achieved most effectively by displacing the resonator downstream with respect to the flow. As follows from (1), a change in the velocity of the mixture while its temperature is constant at the output from the pumping region, does not influence the value of l_π, since the specific input power changes proportionally, while the increase in the carbon dioxide concentration, as noted above, reduces the coefficient η when E/p = const., and for this reason, l_π likewise changes insignificantly. The results obtained,

taking into account the interrelationship of the parameters included in (1) which was noted above, will also apparently be justified at the maximum pumping powers of the laser mixture.

The electron gun developed by L.P. Shanturin and V.I. Fedorov was used in the experiments.

BIBLIOGRAPHY

1. N.G. Basov, V.A. Danilychev, et al., KVANTOVAYA ELEKTRONIKA, 2, 2,458, (1975).

2. Yu.I. Bychkov, V.P. Kudryashov, et al., KVANTOVAYA ELEKTRONIKA, 3, 1,558, (1976).

3. A.V. Artamonov, A.A. Vedenov, et al., KVANTOVAYA ELEKTRONIKA, 4, 184, (1977).

4. A.V. Artamonov, Yu.A. Yegorov, et al., KVANTOVAYA ELEKTRONIKA, 5, 920, (1978).

5. Ye.P. Velikhov, et al., ZHETF [JOURNAL OF EXPERIMENTAL AND THEORETICAL PHYSICS], 65, 543, (1973).

6. K.N. Ul'yanov, Ya.I. Londer, et al., "Trudy 12-y mezhdunarodnoy konferentsii po yavleniyam v ionizovannykh gazakh" ["Proceedings of the 12th International Conference on Phenomena in Ionized Cases"], Eindhoven, Holland, 1975, Part 1, p 176.

7. N.G. Basov, V.A. Danilychev, et al., KVANTOVAYA ELEKTRONIKA, 4, 2,216, (1976).

8. V.P. Popovin, Yu.I. Sholokhov, ZHTF [JOURNAL OF TECHNICAL PHYSICS], 47, 358, (1977).

[173-8225]

8225
CSO: 1862

UC 621.378.33

THE POWER PARAMETERS OF ELECTRON BEAM INITIATED H_2-$F_2D_2F_2$ AND D_2-F_2-CO_2 LASERS

Moscow KVANTOVAYA ELEKTRONIKA in Russian Vol 7, No 6, Jun 80 pp 1357-1359 manuscript received 3 Dec 79

[Article by A.S. Bashkin, A.N. Orayevskiy, V.N. Tomashov and N.N. Yuryshev, Physics Institute of the USSR Academy of Sciences imeni P.N. Lebedev, Moscow]

[Text] A comparative study is made of the lasing in chemical H_2-F_2, D_2-F_2 and D_2-F_2-CO_2 lasers initiated by an electron beam. It is found that under identical experimental conditions, the output energy of a D_2-F_2-CO_2 laser is practically on a par with the output power of a H_2-F_2 laser, where the lasing pulse width of a D_2-F_2-CO_2 laser is 2.5 times greater. Using a mixture of F_2:D_2:O_2:CO_2:He = = 150:60:12:150:375 mm Hg, a specific energy output of 60 J/l was obtained with a chemical efficiency of 3.5 percent and an efficiency with respect to the pumping energy input into the active volume of 330 percent. A slight influence of the He content in the mixture on the lasing parameters of a D_2-F_2-CO_2 laser was detected.

The utilization of a chain reaction of fluorine with hydrogen (or deuterium) in pulsed chaemical lasers makes it possible to obtain high power, high efficiency lasing with HF molecules (λ = 2.7--3.2 μm) and DF molecules (λ = 3.7--4.2 μm), and when the transmission of the vibrational excitation energy is utilized, this lasing can be had with CO_2 molecules also (λ = 10.6 μm). Thus, an energy output of 70 J/l in the lasing mode and 150 J/l in an amplification mode are reported in the literature [1, 5] for a photoinitiated D_2-F_2-CO_2 laser. On the other hand, the utilization of an electron beam for triggering a HF laser

TABLE

(1) Давление компонентов смеси, мм рт. ст.

P_1	H_2	D_2	O_2	CO_2	He	(2) Энергия генерации, Дж	(3) $\varepsilon_л$, Дж/л	$[F]$, 10^{13} см$^{-3}$	η, %	(4) $\eta_{хим}$, %	(5) Квантовый выход генерации, фотон/атом F	(6) $\tau_{имп}$, мкс
50	20		4		125	2,88	24	1,4	900	3,7	260	3--3,5
50		20	4		125	1,2	10	1,4	375	1,6	145	3,5
50		20	4	50	125	2,6	22	1,4	360	3,5	845	8,5--9,5
150		60	12	150	375	7,2	60	4,5	330	3,5	765	3,5

Key: 1. Pressure of the mixture components, mm Hg;
2. Lasing energy, J;
3. Specific energy output, J/l;
4. Chemical efficiency, percent;
5. Quantum lasing yield, photons/atom F;
6. τ_{pulse}, microseconds.

made it possible to obtain lasing with a specific energy output of 100 J/l [2, 3] and even higher [4] with a high electron beam energy conversion efficiency ($\eta \approx 10^3$ %), where this efficiency represents conversion of the energy input into the active volume of the laser to the energy of a lasing pulse [2].

An attempt was made for the first time in [5] to compare the characteristics of high power photoinitiated H_2-F_2 and D_2-F_2-CO_2 lasers. In the lasing mode using CO_2 molecules, a high value was obtained for the specific energy output ($\varepsilon_{las} \sim 70$ J/l), however, in the lasing mode using HF molecules, ε_{las} was low (15 J/l). A comparison of the parameters of H_2-F_2 and D_2-F_2-CO_2 lasers under such conditions can hardly be a correct reflection of the potential capability of a H_2-F_2 laser. The use of pulsed flashlamps as the pumping source likewise makes it difficult to have a real comparison of the energy parameters because of the relatively long pumping pulse width (as compared to the lasing pulse width of an atmospheric pressure H_2-F_2 laser).

This paper is devoted to a study of the parameters of a D_2-F_2-CO_2 laser, excited by an electron beam, and a comparison of these parameters with those for HF and DF lasers under identical experimental conditions. The very small pumping width which was used ($\tau = 25$ ns) makes it possible to assume that it is practically instantaneous as compared to the lasing pulses of both D_2-F_2-CO_2 and H_2-F_2 lasers, something which makes it

possible to relatively simply and precisely determine the degree of initiation.

A detailed description of the installation is given in [6]. The difference consists in the use of NaCl windows and a resonator formed by a copper mirror with a radius of curvature of 47 m and a semitransparent mirror with a dielectric coating, having a reflectivity of 40 percent at a wavelength of 10.6 μm. The active volume of the gaseous medium was 120 cm^3.

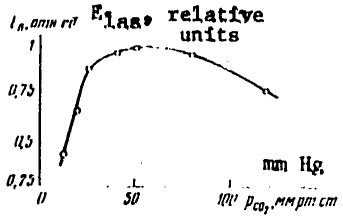

Figure 1. The laser output energy for a mixture of $F_2:D_2:O_2:He:CO_2$ = = 50:20:4:125:p_{CO_2} mm Hg as a function of the CO_2 pressure.

The influence of the composition and pressure of the mixture on the output power and the width and waveform of the lasing pulse were studied. The main data on the mixture compositions which were used and the degrees of initiation and the lasing parameters are given in the Table.

The output energy of the laser is shown in Figure 1 as a function of the CO_2 content in the mixture. The initial linear rise can be explained by the increase in the rate of transmission of the excitation from the DF molecules to the CO_2 molecules. The drop in energy with a high CO_2 content in the mixture cannot be attributed in the usual way to an increase in the autorelaxation and the reduction in the vibrational temperature of the 00^01 mode, since it is observed at small values (≈ 1) of the $[CO_2]/[F_2]$ ratio, while the optimum value of $[CO_2]/[F_2]$ in photoinitiated lasers usually amounts to 2 to 4 [5]. In this case, it is explained as a consequence of the specific features of the pumping source utilized.

Since CO_2 has a high molecular weight, increasing the density of the active medium leads to nonuniform energy losses of the electron beam along the optical axis of the laser, and consequently, to inhomogeneous initiation. Moreover, as has been demonstrated previously [3, 6], the introduction of additives which do not contain fluorine, practically does not increase the degree of initiation.

It is interesting to note that a reduction in the He content in the mixture, right up to its complete absence, did not cause a drop in the

lasing energy. The presence of He made it easier to prepare the mixture, improving its stability (especially if one takes into account the small CO_2 content in our experiment), and also improved the intermixing of the regeants with the sequential admission of the gases. The variation

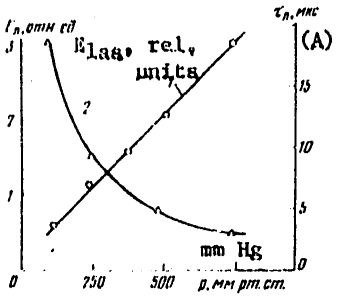

Figure 2. The output energy (1) and the pulse width (2) of a laser using a mixture of F_2:D_2:CO_2:He = = 5:2:5:12.5 as a function of its pressure.

Key: A. τ_{laser}, microseconds.

Figure 3. Oscilloscope traces of the pump pulses (1) and the lasing pulses of H_2-F_2 (2), D_2-F_2 (3) and D_2-F_2-CO_2 lasers (4).

in the D_2/F_2 ratio in the mixture in a range of 0.3 to 1 had a slight impact on the output energy of the laser.

The laser output energy is shown in Figure 2 as a function of the overall pressure of the mixture. A linear rise in the lasing energy was observed with an increase in the mixture pressure, where the upper limit of the mixture pressure (about 1 atm) corresponded to a density of the medium at which linear change in the electron beam absorption energy is observed along the optical axis of the laser. The width of the lasing pulse approximated a p^{-1} law. A specific energy output of ε_{las} = 60 J/l was obtained at the maximum mixture pressure for η_{chem} = 3.5 percent and η = 330 percent.

Oscilloscope traces of the lasing pulses of HF, DF and DF-CO_2 lasers, as well as the pumping pulse are shown in Figure 3. The corresponding data for the mixtures, initiation conditions and lasing parameters are given in the first three lines of the table. It can be noted that the lasing pulses of HF and DF lasers are approximately identical in their waveform and begin immediately following the pumping pulse. The lasing pulse of the D_2-F_2-CO_2 laser though has a delay of 0.6 to 0.8 microseconds relative to the pumping pulse, something which is due to the finite rate of the process of transmitting the excitation from the DF* molecules to the CO_2 molecules, and its waveform is quite reminiscent of the lasing waveform of a TEA CO_2 laser. It must be noted that the lasing pulse width of the D_2-F_2-CO_2 laser is 2.5 times greater than the pulse width of the HF laser.

Working from the data of the table, one can say that for the same level of initiation and an identical pressure of the F_2-$H_2(D_2)$ mixture, the lasing energy of a D_2-F_2 laser is 2.5 times less than that of an HF laser, while the D_2-F_2-CO_2 laser is practically not inferior to the HF laser in terms of energy. For approximately the same chemical efficiency (η_{chem}) as a H_2-F_2 laser, the efficiency in terms of the input energy for a D_2-F_2-CO_2 laser is 2.5 times lower and equal to 350 percent. However, it must be noted that in computing the efficiency, the energy lost by the beam not only in the F_2 molecules, but also in the other components of the mixture, was taken into account. For mixtures of CO_2, the fraction of ineffectively lost beam energy comprises a significant amount. The values of the quantum lasing yield though, ν (see the Table), of a D_2-F_2-CO_2 laser are quite high (about 800) and exceed the corresponding values for the H_2-F_2 laser (ν = 250). If you consider the fact that the beam energy lost only in the F_2 molecules goes for the formation of atomic fluorine, then the efficiency of a D_2-F_2-CO_2 laser amounts to about 800 percent and practically matches the efficiency of an H_2-F_2 laser. This shows that in the case of photoinitiated lasers, where there are no pumping energy losses in CO_2 molecules, the efficiency of both H_2-F_2 and D_2-F_2-CO_2 lasers should be approximately the same.

The value of ν obtained for the D_2-F_2-CO_2 laser substantially exceeds the value of ν = 120 measured in [5]. The quantum yield of the HF laser which was obtained in this paper is three times greater than in [7] and five to six times greater than in [5]. This comparison shows that in our case, with the use of a comparatively weak but very short initiation and carefully prepared working gas mixtures, a long chemical chain length was successfully obtained. All of this attests to the great potential capability of chemical hydrogen fluoride lasers.

Thus, the research indicates that the specific energy outputs of H_2-F_2 and D_2-F_2-CO_2 lasers under the same experimental conditions differ

insignificantly from each other. However, it must be noted that with the use of an electron beam, the presence of a dense gas in the working mixture which does not yield an increase in the yield of atomic fluorine, i.e., such a dense gas as CO_2, leads to the useless expenditure of beam energy. For this reason, the use of photoinitiation is apparently preferable specifically for the D_2-F_2-CO_2 laser, especially if one considers that with the appropriate mixture parameters and initiation levels, the width of the lasing pulse of a D2-F_2-CO_2 laser is 2.5 to 3 times greater than the lasing pulse width of the H_2-F_2 laser, something which makes it possible to reduce the requirements placed on the pumping pulse width.

BIBLIOGRAPHY

1. N.G. Basov, A.S. Bashkin, P.G. Grigor'yev, A.N. Orayevskiy, O.Ye. Porodinkov, KVANTOVAYA ELEKTRONIKA, 3, 2,067, (1976).

2. A.S. Bashkin, A.F. Konoshenko, A.N. Orayevskiy, V.N. Tomashov, N.N. Yuryshev, KVANTOVAYA ELEKTRONIKA, 5, 1,608, (1978).

3. A.S. Bashkin, A.F. Konoshenko, A.N. Orayevskiy, V.N. Tomashov, N.N. Yuryshev, KVANTOVAYA ELEKTRONIKA, 8, 2,166, (1979).

4. R.A. Gerber, E.L. Patterson, J. APPL. PHYS., 47, 3,524, (1976).

5. V.Ya. Agroskin, G.K. Vasil'yev, V.I. Kir'yanov, V.L. Tal'roze, KVANTOVAYA ELEKTRONIKA, 5, 2,436, (1978).

6. A.S. Bashkin, A.F. Konoshenko, A.N. Orayevskiy, V.N. Tomashov, N.N. Yuryshev, "Preprint FIAN" ["Preprint of the USSR Academy of Sciences Physics Institute imeni P.N. Lebedev"], No. 274, Moscow, 1978.

7. N.R. Greiner, IEEE J., QE-9, 1,123, (1973).

[173-8225]

8225
CSO: 1862

MAGNETOHYDRODYNAMICS

UDC 532: 538.4

FLOW IN CHANNELS OF MHD [MAGNETOHYDRODYNAMIC] DEVICES

Moscow TECHENIYE V KANALAKH MGD-USTROYSTV in Russian 1979 signed to press 24 Jul 79 pp 2-5, 363-364

[Annotation, Foreword and Table of Contents from book by A. V. Tananayev, Atomizdat, 1320 copies, 368 pages]

[Text] The book considers laminar and turbulent flows in pipes and channels that determine the operating process in many MHD devices. The principles of the hydrodynamics of viscous incompressible liquid are cited and modern concepts on the structure of the turbulent flow of the wall boundary layer are stated briefly. Preference is given to the consideration of the physical picture of the flow, and the mechanism of the effect of the magnetic field on electrical-conducting liquid (it is assumed that the induced magnetic field is insignificant compared to that applied externally). A great deal of attention in the book is devoted to comparing the results of theoretical investigations with experimental data. In this case, the experimental data, obtained in the Leningrad Polytechnical Institute imeni M. I. Kalinin, part of which is published for the first time, is used widely. Methods are considered for the approximate solution of wall boundary flows (within the framework of the wall boundary layer theory and semiempirical turbulence theory), that make it possible to calculate the hydraulic characteristics of the flow-through channel of MHD devices with an accuracy satisfactory for engineering design.

This book is intended for scientific and engineering-technical workers who develop MHD devices. At the same time, it will be of interest to fluid mechanics engineers and may be used as a textbook on applied magnetic hydrodynamics for students and graduate students in technical VUZ's.

183 figures; 3 tables; bibliography contains 236 items.

Foreword

The interaction between the magnetic field and the flow of an electrical-conducting liquid is exhibited basically in two aspects: in the appearance of volumetric pondermotive forces and in the excitation of the initial magnetic field itself. The totality of the effects produced by these phenomena is the subject of the study of magnetic hydrodynamics. In many applications problems, the effect of the magnetic field is reduced only to the dynamic influence on the flow. But even in this case the volumetric electromagnetic forces produce the formation of complex spatial flows not observed in regular hydrodynamics. The effect of the magnetic field on the turbulence in the conducting media is of special interest. The MHD turbulence, as a phenomenon of nature that determines geophysical and astrophysical processes in many ways, determines in the application aspect the efficiency of various MHD devices and technological processes in power engineering, metallurgy, and in the chemical and mine-enriching industries. Moreover, the magnetic field may influence the flow by a contactless method and thus make it possible to study the fundamental properties of turbulence.

The application aspects of magnetic hydrodynamics acquire a special urgency in connection with the development of scientific-engineering problems of the MHD method of energy conversion and controlled thermonuclear fusion.

The successful start-up of an experimental-industrial 25,000 kw magnetogasdynamic generator was implemented successfully in the USSR. Similar generators are also being created abroad. At present, it may be stated with assurance that it is possible to create powerful electric power plants with MHD generators operating with plasma products of combustion. It may be expected that the efficiency of the thermal cycle of such plants will reach 50 to 55% compared to the 40-42% for the best fossil fuel electric power plants.

Various MHD devices -- pumps, batchers, flowmeters and so forth, find constantly wider usage in various fields: power engineering, metallurgy and transportation installations. Large pumps are being made for AES with fast neutron reactors with liquid metal coolants. In the Tokamak type controlled thermonuclear fusion installations, the use of lithium as a coolant has a number of advantages. In this connection, problems arise of simulating the flow of lithium in the components of the reactor hydraulic system under the effect of a strong magnetic field.

In the general case, processes occurring in the MHD devices are the result of the interaction of four energy flows: hydraulic, magnetic, electric and thermal. It is considered that the greatest share of energy losses in these machines is due to electromagnetic and thermal energies. However, the hydraulic component may reach a value comparable to the other losses. Thus, in electromagnetic pumps, the loss of hydraulic energy may be more than 10 to 40% of the total.

The hydraulic flow in MHD converters is one of the basic interacting flows. Therefore, the approach to an MHD machine as a species of electrical convertor is true only to the first approximation. A more extensive study of the processes occurring in MHD machines indicates that such an approximation is insufficient. The flow structure may also exert a strong effect on electromagnetic phenomena: the velocity distributions and the flow mode (laminar and turbulent) affects the distribution of induced currents, Joule's heat loss, to a great extent which, all things considered, determine the operating efficiency of the entire machine.

In spite of the seeming simplicity of the flow-through channel of most MHD devices, the operating medium may be subjected to complex changes in motion due to the solid boundaries of the flow-through part and the effects of the electrical and magnetic fields. The emphasis on application in the book predetermined the selection of material from a wide number of publications.

A wide group of specialists from various scientific fields, who frequently had no preparation in the hydrodynamics field, is involved in the investigations of MHD problems. Inasmuch as magnetic hydrodynamics is a limited part of general hydrodynamics that uses its methods and results, the book states briefly the principles of the hydrodynamics of viscous, incompressible liquid. In this case, preference is given to the analysis of the physical side of the flow mechanism and where possible, mathematical derivations are omitted. At the same time, however, some approximation methods are considered within the frameworks of the theory of the wall boundary layer and the semiempirical methods of calculating the wall boundary flows. Simple interpolation methods are cited to determine the resistance and velocity distribution of flow, making it possible in many cases to calculate the hydraulic characteristics of the flow-through channel of the MHD machines with an accuracy satisfactory for engineering design.

The wide use is made of research on MHD flows in channels and hydraulic properties of certain MHD devices done at the Leningrad Order of Lenin Polytechnical Institute imeni M. I. Kalinin in the last 15 years under the guidance and with the participation of the author.

These investigations would have been impossible without a great amount of work on creating experimental installations, models, measuring devices, conducting and processing tests which was done by Yu. V. Bogdanov, V. P. Bocheninskiy, A. V. Borisov, N. G. Gontsov, Yu. B. Yemelin, A. I. Kuznetsov, O. A. Marinova, V. G. Marinov, Yu. P. Chernyayev, V. S. Shmarov, V. V. Yakovlev etc. Of great help in preparing the manuscript of the book were Yu. V. Bogdanov, V. P. Bocheninskiy, N. G. Gontsov and V. S. Shmarov; the paper took into account useful comments by N. G. Gontsov, who read the greater part of the manuscript, participated (with Yu. V. Bogdanov) in preparing the material in Chapter 4 and wrote section 4.3. The author expresses his deep gratitude to the persons mentioned.

The author expresses special acknowledgement to N. M. Vekshinskaya and L. V. Marchuk for their work on the makeup of the manuscript.

Contents

[159-2291]

2291
CSO: 1862

NUCLEAR PHYSICS

MEASURING THE ANGULAR DISTRIBUTION OF FLUXES OF PROTONS ESCAPING FROM THE SHIELDING OF A 660-MeV SYNCHROCYCLOTRON

Dubna IZMERENIYE UGLOVYKH RASPREDELENIY POTOKOV PROTONOV, VYKHODYASHCHIKH IZ ZASHCHITY SINKHROTSIKLOTRONA NA ENERGIYU 660 MEV in Russian, Preprint R16-11891, Joint Institute for Nuclear Research, 1978 signed to press 26 Oct 78 pp 1-16

[Paper by V. Ya. Aleynikov, A. R. Krylov, M. M. Komochkov and G. N. Timoshenko, 340 copies, 16 pages]

[Text] A study is done on the differential angular flux density of protons with energies exceeding 43 MeV behind the two-meter concrete shielding of a 660-MeV synchrocyclotron. The ratios of the proton and neutron (more than 20 MeV) components of the radiation field are determined.

The work was done in the Division of Radiation Protection and Radiation Research, Joint Institute for Nuclear Research (JINR).

There may be considerable discrepancies between the results given by various methods used for calculating the parameters of the radiation field behind the shielding of proton accelerators because of the inadequacy of information on the interaction of high-energy particles with the nuclei of the shield material and the use of different kinds of simplifying assumptions in calculating the internuclear cascade. In such a situation, the best method of checking the applicability of a given method of calculation is to compare the calculated and measured field parameters. Ref. 1, 2 give the results of an experimental check on some methods of calculating the integral characteristics of the neutron field (flux, equivalent dose) behind the shielding of a 660-MeV synchrocyclotron with source-shielding configurations typical of accelerators. Our research was done to get experimental information on the differential characteristics of the field, specifically on the angular dependence of the flux density of protons escaping from the accelerator shielding for source-shielding configurations like those in which the integral

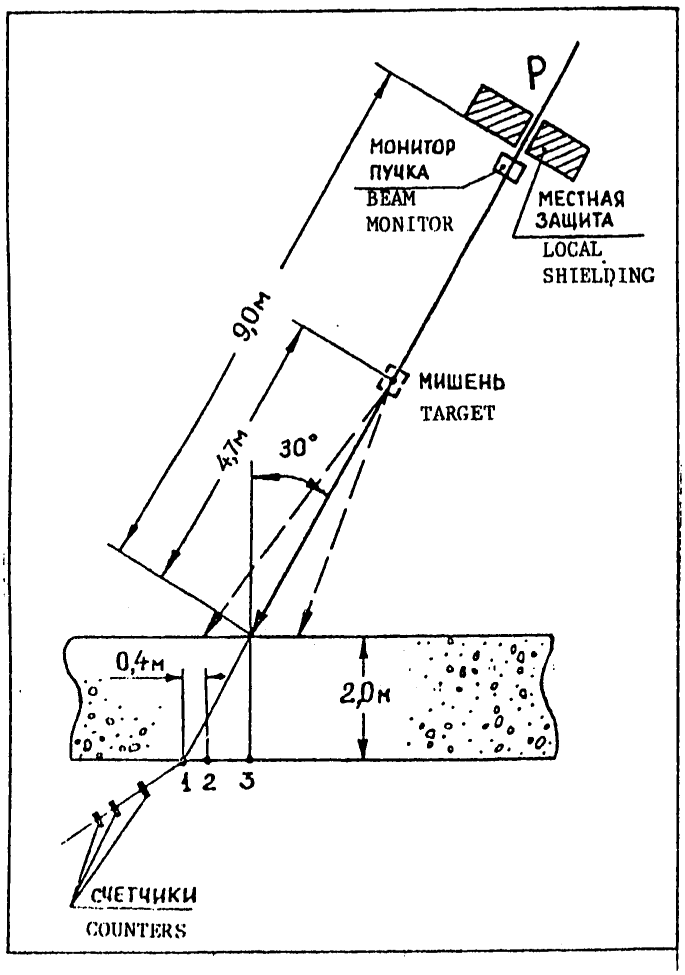

Fig. 1. Measurement geometry

characteristics of the field were studied. Such information is needed not only for checking methods of calculating the field of protons behind the accelerator shielding, but also for correct interpretation of dosimeter readings in these fields.

The measurements were done on the synchrocyclotron of the Laboratory of Nuclear Problems at JINR in two configurations, as shown in Fig. 1. In the first case, a 630 MeV proton beam with intensity of about $6.3 \cdot 10^9$ s^{-1} was incident at an angle of 30° on a two-meter shield of ordinary concrete ($\rho = 2.35$ g/cm^3). The beam was 16 cm in diameter at the point

of incidence. In the second configuration the beam was completely stopped in a copper target 30 cm thick and 12 cm in diameter placed 4.7 m from the shielding on the path of the beam. In the latter case, the source was the radiation generated in the target. The differential angular dependence of proton flux density was determined at three points on the outside of the shield: where the plane of the shield intersects the continuation of the axis of the beam (point 1), where the plane of the shield intersects the normal to the center of beam incidence (point 3), and at point 2 situated between points 1 and 3 at a distance of 40 cm from point 1. Measurements were made of the number of pulses registered by a telescope of scintillation counters with rotation through angles θ and ϕ in the selected coordinate system shown in Fig. 2a. The coordinate origin coincides with the investigated point r_0, plane ZY coincides with the plane of the shield, and $\bar{\Omega}_T$ is the unit vector of the optical axis of the telescope. The count N of the telescope is related to the plane of the proton flux by the following expression:

$$N = \int_S \int_{\Psi(\bar{r})} \Phi(\bar{r},\bar{\Omega})\, dS\, d\Omega, \tag{1}$$

where $\Phi(r,\Omega)\cos\omega$ is the differential angular dependence of the flux of protons with energies from E_{min} to E_{max} at point r on the surface of the shield, ω is the angle between Ω_T and the X-axis, $\Psi(\bar{r})$ is the solid angle in which protons traveling from point $\bar{r}$ in direction Ω will be registered by the telescope, and S is the set of points from which radiation is registered by the telescope. The quantities $\Psi(\bar{r})$ and S depend on the dimensions of the scintillators, the base of the telescope and the geometry of the measurements. Assuming that $\Phi(\bar{r},\bar{\Omega})$ depends weakly on r and Ω within the limits of S, expression (1) can be written in a first approximation as

$$N = \Phi(\bar{r}_0,\bar{\Omega}_T)\cdot\Gamma(\bar{\Omega}_T), \tag{2}$$

where $\Gamma(\bar{\Omega}_T)$ is the geometry factor

$$\Gamma(\bar{\Omega}_T) = \int\Psi(\bar{r})\, dS, \tag{3}$$

For a telescope with scintillators of rectangular shape, the geometry factor can be found in analytical form:

$$\Gamma(\Omega_T) = \frac{4ac}{d\sin^2\omega}\left\{ b\sin\omega\cdot\ln\left|1+\frac{4dl\sin\omega\cdot\cos\omega}{(d\cos\omega - l\sin\omega)^2 - b^2\sin^2\omega}\right| + \right.$$

$$l\sin\omega\cdot\ln\left|1+\frac{4db\sin\omega\cdot\cos\omega}{(d\cos\omega - b\sin\omega)^2 - l^2\sin^2\omega}\right| + \tag{4}$$

$$\left. d\cos\omega\cdot\ln\left|1-\frac{4lb\sin^2\omega}{d^2\cos^2\omega - (l-b)^2\sin^2\omega}\right|\right\},$$

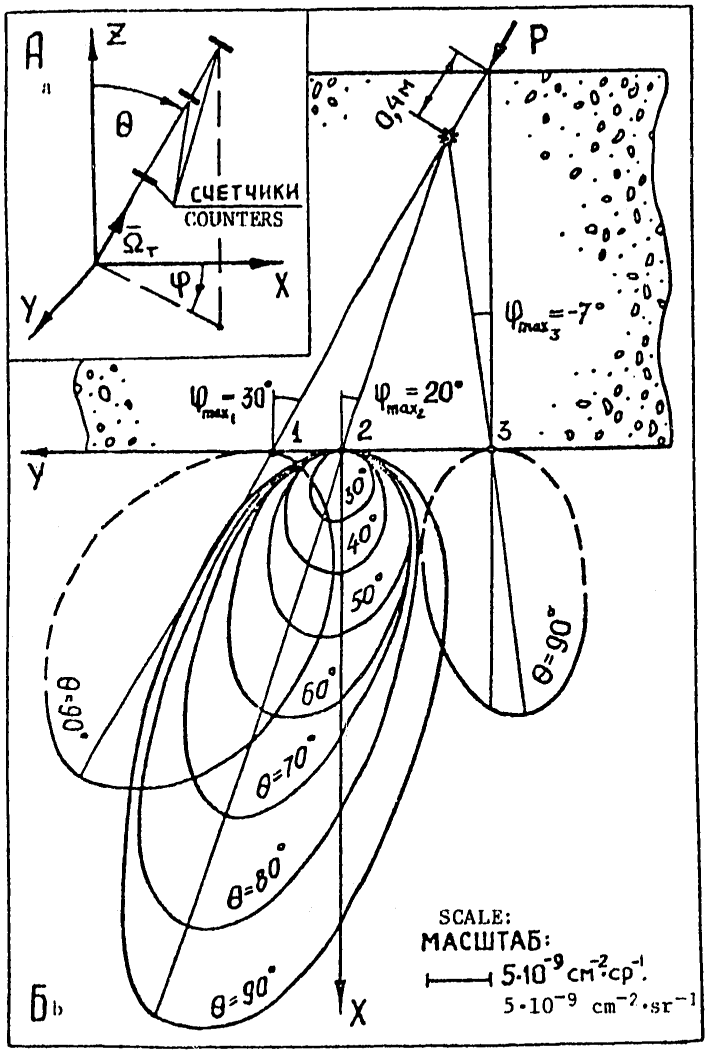

Fig. 2. Directivity patterns of $\Phi(\bar{r}_0,\bar{\Omega}_T)$ for the first configuration

where 2a, 2b are the dimensions of the sides of the scintillator in the first counter (closest to the shield); 2c, 2ℓ are the sides of the scintillator in the third counter (the dimensions of the scintillator in the second counter are selected so that they do not affect the aperture of the telescope); d is the base of the telescope. Sides a and b are

parallel to vector $[X \times \Omega_T]$. The angle ω is related to the angles θ and ϕ by the simple expression

$$\cos\omega = \sin\theta \cdot \cos\phi. \qquad (5)$$

The first assumption that is used in calculating $(\bar{\Omega}_T)$ reduces to the necessity for having a sufficiently small $\Psi(\bar{r})$. For our experiments the value of $\Psi(r) \leqslant 3.0 \cdot 10^{-3}$ sr with angular resolution of the telescope of $\pm 2.9°$. To determine the correctness of the second assumption of weak dependence of $\Phi(r,\Omega)$ on r, measurements were made of the distribution of nucleon flux density Φ_n by carbon-containing activation detectors along the Y-axis on the outside of the shield under conditions of the first source-shield configuration. In doing this, it was assumed that there was little change in the ratio between the neutron and proton components of the field at the investigated points. In this way, the resultant dependence $\Phi_n(Y)$ could be interpreted as the distribution (in relative units) of $\Phi(\bar{r})$, where r are the coordinates of the point along the Y-axis. The maximum dimension of S along the Y-axis is 8.4 cm. It can be

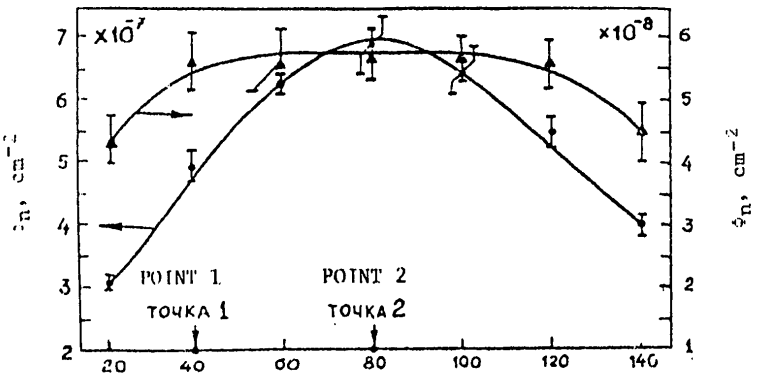

Fig. 3. Distribution of the flux density of nucleons along the Y-axis: ϕ--first configuration ϕ--second configuration

seen from Fig. 3 that for the first configuration the change in $\Phi_n(Y)$ in the vicinity of point 2 is less than 1% within the limits of S, and in the vicinity of point 1 the change is less than 7.5%. The curve is drawn by graphic interpolation through the experimental points within the limits of the random errors indicated on the figure. The systematic error in determination of Φ_n is ~20%.

In determining $\Phi(r_0,\Omega_T)$ it was assumed that the count of the telescope is equal to the number of protons passing through it with energy of

>43 MeV. In reality the telescope count in the radiation field behind the shielding is due to the passage of protons, electrons and pions with sufficient mean free path in the scintillation material, and to random coincidences. Estimates show that the fraction of the pion component of the field in the overall flux is less than 2%. To determine the contribution to the telescope count from the electron field component with energies greater than 3.5 MeV (the energy threshold of the telescope for electrons), measurements were made with an absorber placed in front of the last counter. This increased the electron threshold to 9.5 MeV, and the proton threshold to 68 MeV. The reduction in telescope count was 14.3%. Apparently the major part of this reduction fell to the proton component of the field. There are negligibly few electrons with energies of more than 10 MeV in the overall flux. The maximum contribution of random coincidence did not exceed 1% of the count. On this basis we can assume that 90% of the count of the telescope is due to the proton component of the field. According to estimates, the percentage of registered protons caused by interaction of the neutron component with the material of the first scintillator does not exceed 2% in the worst case.

The values of $\Phi(r_0,\Omega_T)$ found on the basis of (2), which represent the number of protons in the energy range from 43 MeV to 630 MeV passing through an area of 1 cm^2 on the surface of the shield at point r_0 in 1 s in a solid angle of 1 sr in a direction near Ω_T were normalized to one proton incident on the shielding. The flux density of primary neutrons was measured with accuracy of ¿20%? Fig. 2b shows directivity patterns of $\Phi(r_0,\Omega_T)$ as a function of θ and ϕ for three points in the first source-shield configuration. The values of $\Phi(r_0,\Omega_T)$ for the angles shown by the broken lines on the figure were not measured in the experiment. The angular dependence at point 2 was studied in most detail with a step of 15° with respect to ϕ and 10° with respect to θ. The values of ϕ_{max1}, ϕ_{max2}, ϕ_{max3} at which the functions $\Phi(90°,\phi)$ at each investigated point assume maximum values determine the $\Omega_{T_{max}}$ through which passages converge in some small volume within the shielding. This fact can be interpreted as the existence of an "effective" neutron source that forms a proton field component in the last layers of the shield in the case of the first configuration.

Fig. 4 shows curves of $\Phi(\theta,\phi)$ at point 2 in the first source-shield configuration (solid lines). Errors due to statistical errors of telescope counts are indicated on the figure. It can be seen that the curves are not symmetric relative to angles θ and ϕ in the selected coordinate system. There is approximate axial symmetry within limits of 20% relative to the axis X' obtained by rotating the coordinate system about the Z-axis through angle ϕ_{max2}. In doing this, it is assumed that the function $\Phi(\theta,\phi)$ is symmetric relative to the XY-plane. As angle θ decreases, the asymmetry of the relation $\Phi(\phi)$ relative to $\phi = 0$ (the X-axis) becomes less noticeable. This is because more protons formed by quasielastic interactions of nucleons with the shielding material are traveling in the direction determined by ϕ_{max2} and θ_{max2}, and it is primarily cascade protons that escape at small θ as compared with quasielastic protons.

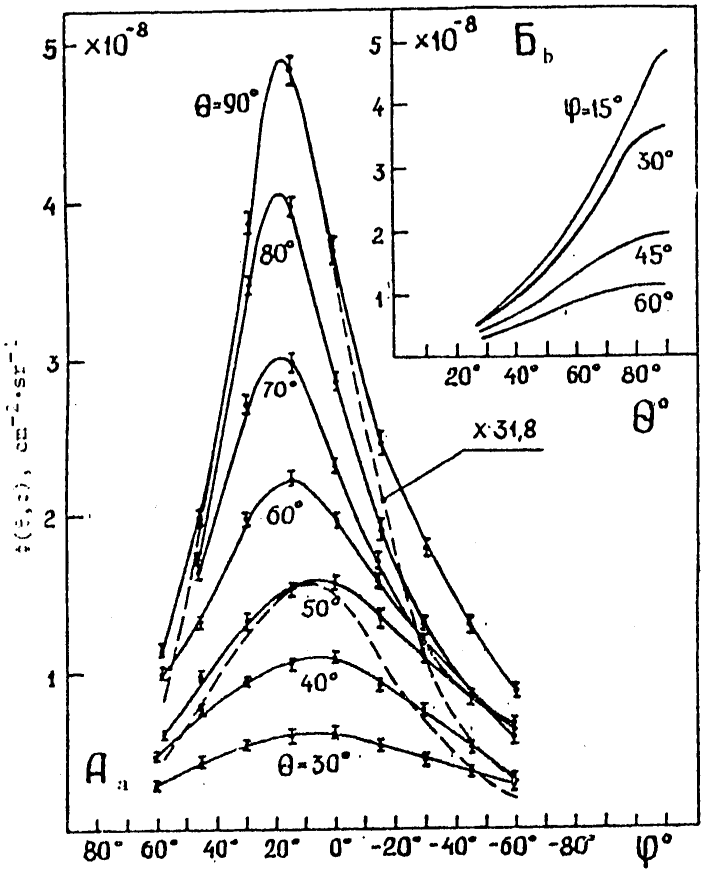

Fig. 4. Curves for $\Phi(\theta,\phi)$: —— first configuration; --- second configuration

This leads to attenuation of the influence that the direction of motion of the original particles has on $\Phi(\theta,\phi)$ at small θ.

The greater absolute values of the differential angular flux densities of protons at point 2 as compared with point 1 can apparently be attributed to the fact that the distances from the point of nucleon production on most of the "core" of the cascade to point 2 are shorter than to point 1, which is equivalent to a thinner shield in the direction to point 2. At the same time, despite the fact that the thickness of the shielding in the direction of point 3 from the point of beam incidence is minimum, a relatively low percentage of nucleons leave the "core" of the cascade at large angles, and the absolute values of $\Phi(\theta,\phi)$ at point 3

are lower than at points 1 and 2. This agrees with the measured distribution of $\Phi_n(Y)$. It can be seen from Fig. 3 that the nucleon flux density at point 2 is approximately 1.5 times as high as at point 1.

Assuming that backscattering of nucleons in air behind the shield is insignificant, and approximating $2\Phi(30°,\phi)\cos\phi$ linearly to 0, we can find the fluence Φ of protons with energies greater than 43 MeV at point 2:

$$\Phi = \int_0^{2\pi} \frac{\Phi(\bar{\Omega})}{\cos\omega}\, d\Omega = 8.58\cdot10^{-8}\ \text{cm}^{-2}.$$

This value of Φ is normalized to one proton incident on the shielding. The percentage of protons in the overall flux is (11.1 ± 2.2)%.

The second configuration, because of the large distance from target to shielding, is an approximate model of a flat unidirectional source of emission. Ref. 2 gives energy spectra calculated by a Monte Carlo method for relativistic neutrons formed in the given target with 660-MeV incident protons in angular intervals of 0-30°, 30-60° and 50-90° relative to the direction of the proton beam. Fig. 5 shows the distributions

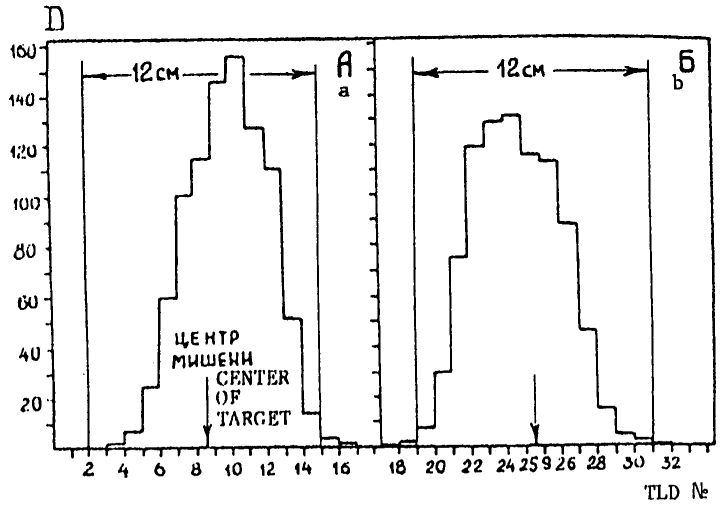

Fig. 5. Distributions of absorbed doses D on the front surface of the target in relative units vertically (a) and horizontally (b)

of absorbed doses on the forward surface of the target along the vertical (Fig. 5a) and along the horizontal (Fig. 5b), as measured by thermoluminescent dosimeters (TLD). At least 99.2% of the protons were incident on the target. According to measurements, the contribution to the count

of the telescope due to background radiation from the local shielding and the enclosed collimmator, and also from the background of the experimental hall is 5.7%.

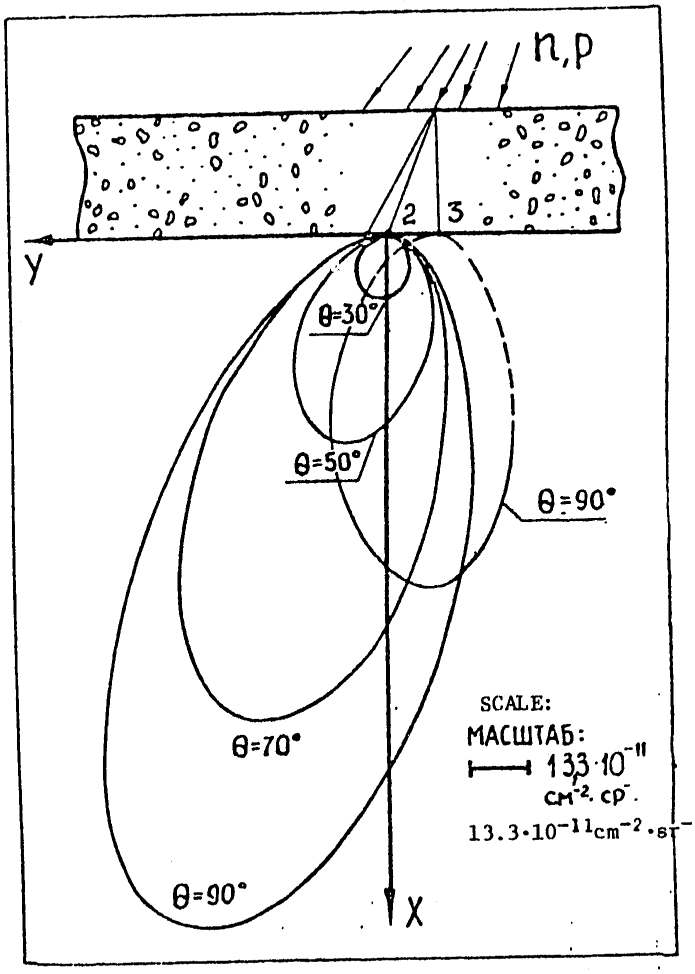

Fig. 6. Directivity patterns of $\Phi(\bar{r}_0, \bar{\Omega}_T)$ for the second configuration

Directivity patterns of $\Phi(r_0, \bar{\Omega}_T)$ as a function of θ and ϕ are shown in Fig. 6. The absolute values of $\Phi(\theta, \phi)$ in the given case are considerably less than in the first configuration; however, the form of the curve for $\Phi(\theta, \phi)$ is approximately the same since in either case the angular

distribution of protons escaping from the shield is formed by the angular distributions of cascade and quasielastic protons escaping from the nuclei of the shielding as a result of nuclear reactions. Shown in Fig. 4 for comparison are $\Phi(90°,\phi)$ and $\Phi(50°,\phi)$ (broken lines) measured in the second configuration and normalized with respect to the maximum of $\Phi(90°,\phi)$ in the first configuration. The greatest discrepancy is observed for values of ϕ close to ±60°. This can be attributed to the fact that the proton spectrum close to the surface of the shielding in the second configuration is "softer," and the percentage of protons that leave the shield at large ϕ and completely lose their energy due to ionization losses increases. The distribution of nucleon flux density along the Y axis in the second configuration is shown in Fig. 3. In this case the distribution of $\Phi_n(Y)$ is a weakly variable function. The fluence of protons with energies greater than 43 MeV at point 2 is equal to $2.5 \cdot 10^{-9}$ cm^{-2}, and the precentage of protons in the overall flux is (3.8 ± 0.8)%. The reduced percentage of protons in the overall nucleon flux becomes understandable if we take into consideration the relative "softness" of the nucleon spectrum in the second configuration. Our data agree well with the ratio of proton and neutron components of the field (3%) behind a shield of 500 g/cm^2 of concrete as found from the results of Ref. 3.

The authors thank G. Ya. Kaskanov, V. P. Bamblevskiy, V. A. Kulikov and A. N. Rezunak for assistance in doing the experiments.

REFERENCES

1. V. E. Aleinikov, M. M. Komochkov, V. I. Tsovboon, "Proc. Intern. Cong. on Protection Against Accelerator and Space Radiation," Vol. 1, p 282, CERN, 71-16, 1971.

2. V. Ye. Aleynikov, M. M. Komochkov, V. P. Kryuchkov, "Trudy VI Vsesoyuznogo soveshchaniya po uskoritelyam zaryazhennykh chastits" [Proceedings of the Sixth All-Union Conference on Charged Particle Accelerators], Moscow, 1974, Vol 11, p 226, 1975.

3. Ye. K. Gel'fand et al., "Trudy radiotekhnicheskogo instituta AN SSSR" [Proceedings of the Radio Engineering Institute, USSR Academy of Sciences], No 22, p 242, 1975.

6610
CSO: 8144/1615

MEASUREMENTS OF SPATIAL DISTRIBUTION OF BREMSSTRAHLUNG DOSE ON THE SILUND ELECTRON INJECTOR OF A COLLECTIVE-ION ACCELERATOR

Dubna IZMERENIYA PROSTRANSTVENNOGO RASPREDELENIYA DOZY TORMOZNOGO IZLUCHENIYA NA INZHEKTORE ELEKTRONOV 'SILUND' KOLLEKTIVNOGO USKORITELYA TYAZHELYKH IONOV in Russian, Preprint R16-11934, Joint Institute of Nuclear Research, 1978 signed to press 27 Nov 78 pp 1-16

[Paper by G. V. Dolbilov and V. I. Tsovbun, 340 copies, 16 pages]

[Text] Studies were done on the radiation characteristics of the SILUND acceoerator, an electron injector for a collective-ion accelerator. The purpose of the work included determining the source function of the collective-ion accelerator as an extended object, and determination of radiation loads on a number of accelerator components. Measurements were done on the SILUND accelerator and on the charged torus generator (compressor) under conditions of capture of an injected electron beam with energy of 1.5 MeV. TLD-100 thermoluminescent detectors based on LiF were used as the dosimeters. The distribution of electron losses in the transfer system between the SILUND injector and the compressor was reconstructed from the dosimeter readings by a method of statistical regularization. The radiation loads on accelerator components were determined, and particularly those on the acceleration tube. Numerical estimates were made of bremsstrahlung dose rates near the collective-ion accelerator in the electron-capture mode. A comparison of calculations with measurement results shows the feasibility of evaluating the radiation environment near a collective-ion accelerator with 50% accuracy when using known parameters for engineering calculations.

The work was done in the Department of New Acceleration Methods at the Joint Institute for Nuclear Research.

This research was done to determine the source function of an extended object, a collective-ion accelerator [Ref. 1], and also to evaluate the radiation loads on a number of accelerator components whose service life is determined in great measure by the effect of ionizing radiation. The collective-ion accelerator consists of two major parts: the SILUND electron accelerator, and the charged torus generator (compressor). Details of the collective-ion accelerator and its major components are described in Ref. 1-2. In our research, the SILUND is the main object of study, and the compressor is considered only in the mode of injected beam capture.

CONDITIONS OF THE EXPERIMENT

The measurements were made with LTD-100 thermoluminescent detectors made by the Harshaw Company on the basis of LiF single crystals [Ref. 3]. Fig. 1 shows an intersectional junction of the SILUND accelerator, and the compressor [Ref. 1-2], and also indicates the placement of the detectors. The numbers 1-4 denote detectors, which are located on the surface of all 5 accelerating sections of the SILUND. In the middle of the second, fourth and fifth sections are vertical holders that each accommodate three detectors, separated by a distance of 20 cm. Information from the detectors in positions 5-6 was used to evaluate the radiation load on the outer surface of the acceleration tube and the magnetic field coil. Four of these detectors were installed on the surface of the acceleration tube at intervals of every 90°. The detectors in position 7 close to the Rogowski loop record the radiation load on the outside of the magnetic field coils and on the epoxy potting compound; the readings of these detectors could also be used to evaluate the radiation load on the ferrite rings of the inductors. All along the accelerator at a height of about 50 cm were detectors to record the radiation dose over the intersectional junctions and over the junction section between the SILUND and the compressor.

The working mode of the accelerator involved capture of the injected beam into the compressor and subsequent transfer into the inflector [Ref. 2]. The measurements were made in two sessions at different times. The measurements differed in details of accelerator adjustment and beam alignment; in the second session, a new acceleration tube had been installed in the third section. The radiation environment in these measurements was also different in details; however, an attempt was made in the work to ascertain the general characteristics of the radiation environment.

Typical oscillograms of the beam current registered by Rogowski loops at the output of the five accelerating sections of the SILUND are shown in Fig. 2 (second measurement session). The last oscillogram shows the total voltage pulse applied to the inductors of all five sections. The time of detector irradiation was about an hour at a current pulse recurrence rate of 0.5 Hz.

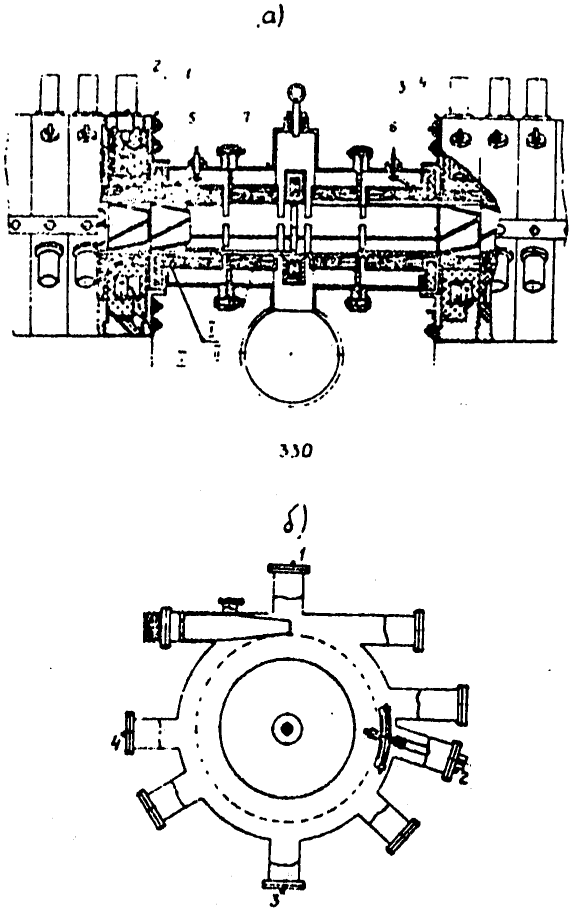

Fig. 1. a) Intersectional junction of the SILUND accelerator; 1-7--placement of detectors; I--acceleration tube; II--magnetic field coils; III--ferromagnetic inductor core; b) compressor; 1-4--placement of the detectors

MEASUREMENT RESULTS AND THEIR ANALYSIS

The distribution of bremsstrahlung dose rates over the outside of the SILUND inductors is shown in Fig. 3. The low levels of the dose rates show that the radiation load on the insulators of the high-voltage connectors and the insulation of live conductors will not determine their

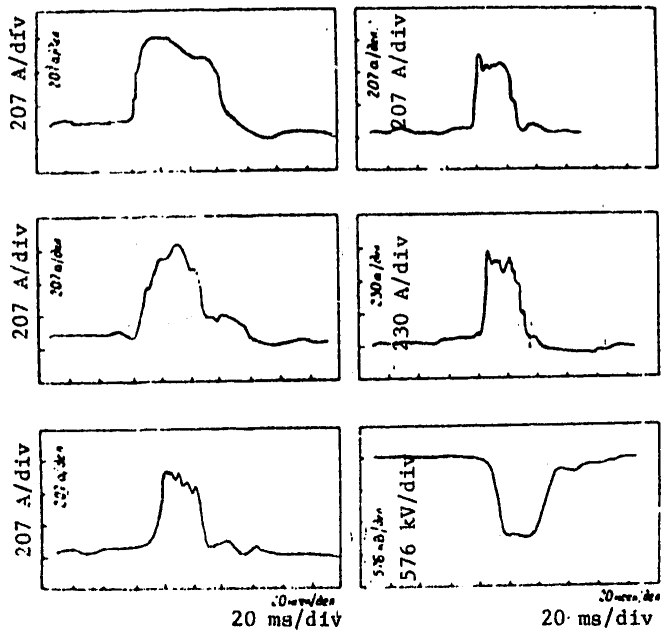

Fig. 2. Typical oscillograms of electron beam current at the output of the five SILUND accelerating sections, and the total accelerating voltage pulse across the inductors of the accelerator

service life. The increased dose rates near the flanges of the accelerating sections are due to irradiation of the detectors on the part of the less shielded junction sections. The dotted curve over the third accelerating section represents the distribution of dose rates on the surface of the section after replacement of the acceleration tube. The readings of detectors on the vertical holders are indicated on the graph by vertical line segments. The arrows indicate that the upper detectors registered a higher dose rate. This means that the radiation passing from the acceleration tube through the inductors does not entirely determine the radiation load on the surface of the inductors, and that scattered radiation makes a considerable contribution to the dose rate at these points.

The bremsstrahlung dose rates at a distance of 50 cm from the accelerator axis are indicated in Fig. 3 by the solid curve (measured in the second session). This information is useful for the case where unforeseen energizing of the accelerator may occur. The 50 cm distance is typical for servicing personnel [Ref. 4]. At a distance of 50 cm it is

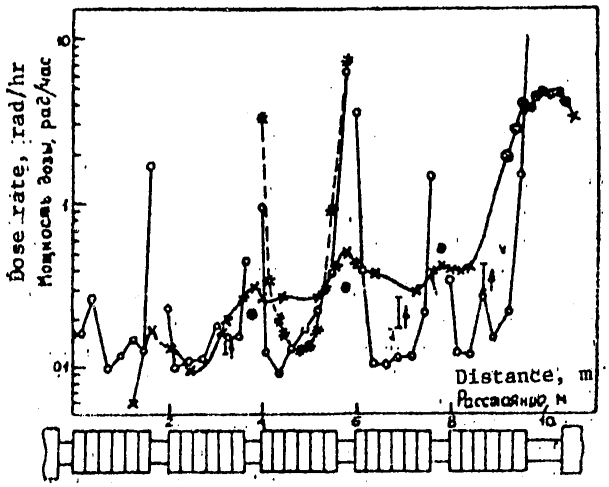

Fig. 3. Spatial distribution of dose rates on the SILUND accelerator: ----o---- -- on the surface of the accelerating sections; ----x---- -- at a height of 50 cm from the axis of the accelerator; ⊛ -- detector readings used to reconstruct electron beam losses; ● --calculated estimates of dose rates above straight intervals at a height of 50 cm

permissible to consider an acceleration tube and electron transfer channel with radii of 30 and 23 mm respectively as linear radiation sources.

The results of measurements on the injector of the collective-ion accelerator enable us to represent it as a source of radiation in the form of intersectional junctions and an electron transfer channel between the SILUND and the compressor. The radiation of other parts of the injector can be disregarded in evaluating dose rates at some distance from its axis.

The black circles in Fig. 3 show numerical estimates of the dose rates at a height of 50 cm above the intersectional junctions. The initial data for these estimates were electron beam losses determined from the difference in areas under oscillograms of the beam current at the output of each section, and the electron energy at the output of the sections. The increase in energy of electrons with acceleration in one section was about 275 keV, and the electron gun injection energy was 200 keV. Electron losses were averaged uniformly over the length of two adjacent sections, and the percentage of losses on an intersectional junction was taken as proportional to its length. The losses were assumed to be localized in the center of an intersectional junction. The angular

distributions of bremsstrahlung dose rate for materials with low atomic weight were taken from Ref. 5.

The lengthwise distribution of electron losses in the electron transfer channel between the SILUND and compressor was reconstructed from the readings of detectors (symbolized by ● in Fig. 3) placed above this channel. Reconstruction was done by a method of statistical regularization [Ref. 6] using a program described in Ref. 7-8. If S(z) denotes the losses of electrons in region z on a unit of length of the electron transfer channel, then the bremsstrahlung dose rate measured by the TLD is determined from the expression

$$(D+\delta)_{i=1,9}=\int_0^{z_{max}} S(z)\cdot\frac{P(\theta_i)}{R_i^2(z)}\cdot dz, \qquad (1)$$

where $P(\theta_i)$ is the angular distribution of bremsstrahlung dose rate [Ref. 8], θ_i is the angle between the direction of motion of electrons and the direction of the radiation to the i-th detector from point z, $R_i(z)$ is the distance to the i-th detector from point z, δ_i is the error in determination of the dose rate by the i-th detector.

A similar problem was solved in Ref. 9 for proton losses on the beam extraction channel from a synchrophasotron. In this case it was necessary to demonstrate the feasibility of finding losses from equations (1) with kernel $P(\theta_i)/R_i^2(z)$, which was done by trial reconstruction of predetermined losses. System of linear equations (1) was solved after linearization

$$(D+\delta)_{i=1,9}=\sum_{j=1}^{30} S(z_j)\frac{P(\theta_i)\cdot Nz_j}{R_i^2(z)}. \qquad (2)$$

Here $Nz_j = 5$ cm, $z_{max} = 110$ cm. The error $\delta_i = \pm 20\%$ for $i = 1.8$ and $\delta_{1.9} = \pm 30\%$. According to our estimates (see below), the contribution to the radiation dose measured by the 9-th detector from electrons captured into the compressor and transferred into the inflector was less than 30%. This contribution was much less for the other detectors.

The results of reconstruction of the distribution of electron losses in the electron transfer channel, and the "corridor" of errors of reconstruction are shown in Fig. 4. This figure also shows the way that electron losses depend on the length of the selected section of the channel:

$$R(z_0)=\frac{\int_{z_0}^{z_{max}} S(z)\cdot dz}{\int_0^{z_{max}} S(z)\cdot dz}.$$

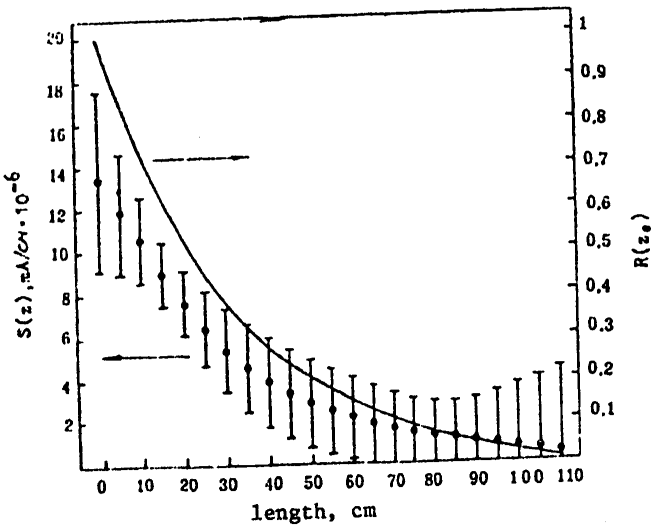

Fig. 4. Distribution of electron losses with respect to length of the electron transfer channel

The detector readings reconstructed from the calculated loss distribution correspond to the initial readings within the limits of the errors δ_i. The decreasing behavior of losses is due to titanium foil placed at the end of the fifth section to separate the vacuum sections of the SILUND and the compressor, and also by a reduction in the aperture of the channel at this point from 60 to 47 mm. The total losses of average current on the transfer channel amounted to 0.44 μA.

As an example, Fig. 5 shows the dose rates registered by detectors on the surface of the acceleration tube in the vicinity of the second and third sections for the two measurement sessions. The spatial distributions of dose rate on the surface of the acceleration tube indicate localization of losses of a helically moving electron beam, and may be useful for correcting accelerator alignment. The results of measurements of the dose rates at four points on the compressor (Fig. 1) were also compared with numerical estimates. It was assumed that an electron beam with the current measured by the Rogowski loop at the output of the fifth section with deduction of losses on the electron transfer channel was injected into the compressor, and after capture was transferred to a stainless steel inflector. The direction of motion of the electrons upon impact against the inflector was close to the tangent of a circle drawn from the center of the compressor with radius equal to the distance to the nearest point of the inflector. The energy of the injected electrons was 1.5 MeV. In the calculations, consideration was taken of attenuation of

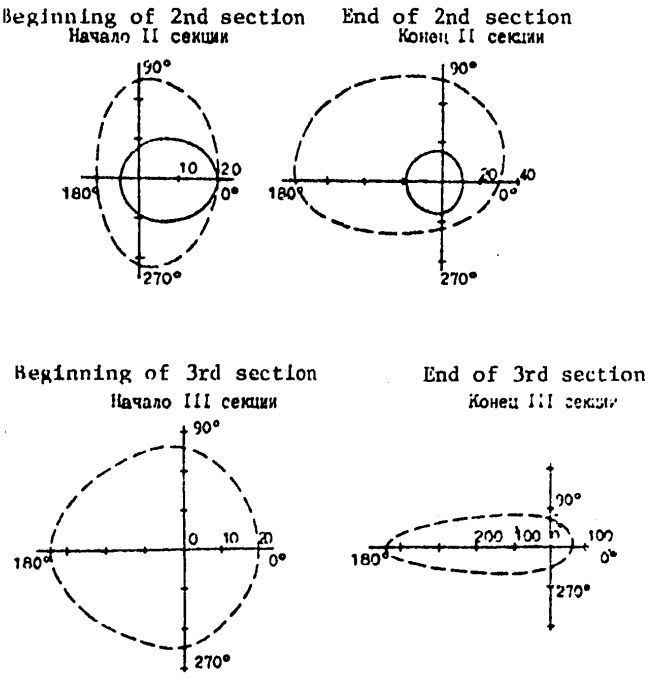

Fig. 5. Dose rates (rad/hr) recorded on the surface of the acceleration tube of the SIGUND: -- first session; --- -- second session

radiation in components of the chamber and the compressor stand on lines connecting the point of beam loss and the points of detector installation. As a rule the absorber was of compound construction and consisted mostly of stainless steel and glass-textolite. The attenuation parameters for a wide beam of bremsstrahlung in concrete expressed in cm^2/g were taken from Ref. 10. The results of calculation of dose rates in rad/hr with the accepted assumptions are summarized in Table 1 as compared with measurement results. The figures in parentheses in the table are the results of calculation without consideration of beam attenuation in the components of the electron ring compressor.

TABLE 1

Point No		1	2	3	4
Measurements	1	27	5.4	1.6	--
	2	48.3	9	3.6	5.6
Calculation	1	21.8 (47.4)	3.4 (19.5)	1.8 (3.8)	--
	2	36.8 (80)	5.7 (33)	4.2 (9)	2.9 (8.6)

The radiation dose measurements given in this paper are for the absorbed dose in the TDL, which is close to the absorbed dose in biological tissue, organic materials and materials with low atomic weight. The measurement error (about 15%) is due mainly to the spread of sensitivities of detectors in a batch.

Comparing calculations and measurements, we can state that the described idealized representations of a collective-ion accelerator as a source of radiation under operating conditions of capture of the injected beam enable relatively simple numerical evaluations of the radiation environment close to an accelerator with 50% accuracy when using known parameters for engineering calculations.

RADIATION LOADS ON ACCELERATOR COMPONENTS

The objects studied for radiation loads are summarized in Table 2. In using the handbook data [Ref. 11-14], the absorbed doses of gamma radiation leading to losses of 50% of the mechanical or electrical properties

TABLE 2

Object	Material	Radiation resistance limit, rads		Radiation load, rad/hr
1. Acceleration tube a) outside b) inside	Pyroceram, ceramic	10^9		2-450 $2 \cdot 10^6$
		Impact strength	Electric strength	
2. Magnetic field coils	Polymethyl methacrylate	$6 \cdot 10^7$	10^8	2-450
	K-115 epoxy compound	$7 \cdot 10^9$	$4 \cdot 10^8$	
3. Inductor a) insulator	K-115 epoxy compound	$7 \cdot 10^9$	$4 \cdot 10^8$	0.4-10
b) ferrite rings	ferrite	10^9		0.4-10
4. Vacuum seals	7889 vacuum rubber	$8 \cdot 10^7$		2-450

of the material were taken as the limit of radiation resistance of the given material.

The work life of the acceleration tube with radiation exposure is an important characteristic of induction accelerators, which may limit the maximum electron beam current and the duration of accident-free accelerator operation [Ref. 16]. Therefore the radiation loads on the acceleration tube were considered in greater detail. The measurements were done on the outside of the acceleration tube, and numerical estimates were made for its inner surfaces. The estimates were made for the tube segment of the fourth accelerating section. The average kinetic energy of electrons was about 1 MeV, and losses were evaluated by means of oscillograms, and amounted to $7.5 \cdot 10^{12}$ el./s. It was assumed that the losses were uniformly distributed, and that the average loss density was $2 \cdot 10^{9}$ el/cm^2·s. The estimate used calculations of the energy release in a flat semi-infinite layer of carbon with incidence of 1 MeV electrons at an angle of 89° to the normal done by Berger [Ref. 17]. According to Berger, the energy release was tens of MeV·g/el./cm^2 close to the surface, and decreased by a factor of tens at a depth of 0.1 g/cm. In our case, this corresponds to a radiation load of about 2 Mrad/hr near the inner surface of the acceleration tube. Radiation heating of the inside of the tube in this case is about 0.01°C per current pulse. It is noteworthy that for a wall thickness of 18 mm in the acceleration tube, the change in the radiation load from inside to outside is about four orders of magnitude.

In alignment of the accelerator, local electron losses may be 3-4 orders greater than the density of losses estimated above, and the temperature difference between the surfaces of the inside and outside of the acceleration tube may reach hundreds of degrees at the instant of completion of the electron current pulse. Mechanical shocks due to nonuniform thermal expansion of the tube material may lead to microcracks and eventual loss of electrical, vacuum and mechanical strength.

Among the other components of the accelerator, those with the shortest radiation life are components in contact with the acceleration tube, and also the magnetic field coil core and vacuum gaskets. The dose load on the ferrite was evaluated with a correction equal to the ratio of the coefficients of absorption of photon energy in ferrite and LiF.

When the SHUND operates on high frequencies [Ref. 16], the radiation loads may increase a hundred-fold, and of course the radiation lifetime of a number of accelerator components will determine the working time of the accelerator without replacement of parts. In this connection it is useful to look for more radiation-resistant substitute materials, and to reduce beam losses, especially during alignment of the accelerator.

In conclusion the authors thank G. V. Maslennikov for assisting with the measurements.

REFERENCES

1. L. S. Barabash et al., Joint Institute of Nuclear Research (JINR), R9-7697, Dubna, 1974.

2. V. P. Sarantsev, E. A. Perel'shteyn, FIZIKA PLAZMY, Vol 3, No 3, 1977, pp 449-464.

3. M. Frank, V. Shpol'ts, "Tverdotel'naya dozimetriya ioniziruyushchego izlucheniya" [Solid-State Dosimetry of Ionizing Radiation], translation from the German, Atomizdat, Moscow, 1973.

4. J. R. Parker, M. J. Engelke, "Proc. of the Int. Conference on Protection Against Accelerator and Space Radiation," Vol 2, CERN, Geneva Switzerland, April 26-30, 1971, p 283.

5. V. I. Tsovbun, JINR, 16-7104, Dubna, 1973.

6. V. F. Turchin, V. P. Kozlov, M. S. Malkevich, USPEKHI FIZICHESKIKH NAUK, Vol 102, 1970, p 354.

7. L. S. Turovtseva, V. F. Turchin, Preprint No 30, Institute of Problems of Mechanics, Moscow, 1971.

8. V. Ye. Aleynikov, V. P. Gerdt, M. M. Komochkov, JINR, R16-8176, Dubna, 1974.

9. V. Ye. Aleynikov et al., JINR, 16-8583, Dubna, 1975.

10. V. I. Tsovbun, JINR, R16-7834, Dubna, 1974.

11. N. A. Sidorov, V. V. Knyazev, editors, "Radiatsionnaya stoykost' materialov radiotekhnicheskikh konstruktsiy. Spravochnik" [Radiation Resistance of Materials in Electronic Equipment. A Handbook], Sovetskoye radio, Moscow, 1976.

12. V. N. Bykov, S. P. Solov'yev, editors, "Vliyaniye oblucheniya na materialy i elementy elektronnykh skhem" [Effect of Irradiation on Materials and Components of Electronic Circuits], Atomizdat, Moscow, 1967.

13. V. B. Dubrovskiy (ed), "Radiatsionnaya stoykost' materialov. Spravochnik" [Radiation Resistance of Materials. A Handbook], Atomizdat, Moscow, 1973.

14. V. Ye. Borodin et al., Preprint LRI 76-140, Institute of High-Energy Physics, Serpukhov, 1976.

15. V. M. Katayev, V. A. Popov, B. I. Sazhin, editors, "Spravochnik po plasticheskim massam" [Handbook on Plastics], Vol II, Khimiya, Moscow, 1975.

16. Yu. P. Vakhrushin, A. I. Anatskiy, "Lineynyye induktsionnyye uskoriteli" [Linear Induction Accelerators], Atomizdat, Moscow, 1978.

17. "RSIC Computer Code Collection," CCC-107, Oak Ridge, 1969.

[8144/1613-6610]

6610
CSO: 8144/1613

INVESTIGATION OF THE ENERGY DISTRIBUTION OF FLUENCE AND NEUTRON DOSE AT LARGE DISTANCES FROM ACCELERATORS

Dubna ISSLEDOVANIYE ENERGETICHESKOGO RASPREDELENIYA FLYUYENSA I DOZY NEYTRONOV NA BOL'SHIKH RASSTOYANIYAKH OT USKORITELEY in Russian, Joint Institute of Nuclear Research, R16-12078, 1979 signed to press 19 Apr 79 pp 1-12

[Paper by M. M. Komochkov, B. V. Man'ko, B. S. Sychev and A. L. Shishkin, 360 copies, 12 pages]

[Text] It is shown that accelerators can be represented by a superposition of point sources with a spectrum close to the actual secondary neutron spectrum on the outer surface of the accelerator shielding in calculations of the energy distribution of fluence and neutron dose at large distances away. For example the Laboratory of Nuclear Problems at the Joint Institute for Nuclear Research (JINR) has used models of an upwardly monodirectional point source and a source with isotropic emission into the upper hemisphere for the synchrocyclotron. A comparison of calculations with the results of measurements of the fluence and neutron dose near the synchrocyclotron has confirmed the validity of the choice of models, and has enabled determination of the parameter of anisotropy of such a source, as well as the contribution of neutrons with energy of more than 20 MeV to the total equivalent neutron dose at great distances from the accelerator. It is noted that using expressions proposed by some authors for describing the way that equivalent dose depends on distance may lead to considerable errors in the estimates of individual doses.

The work was done in the Division of Radiation Safety.

INTRODUCTION

The concepts of radiation risk [Ref. 1] and nonthreshold action of ionizing radiation on people [Ref. 2] make it necessary to consider and

monitor radiation levels and doses that are not only commensurate with the permissible values, but also much lower. The consideration of small individual doses is especially important when large groups of people are subjected to irradiation. To some extent, a situation of this kind can occur at JINR, where the synchrocyclotron and synchrophasotron are capable of producing radiation fields with noticeable levels at considerable distances.

A number of papers have dealt with measurements and estimates of fluence and neutron dose at great distances (see for example Ref. 3-13). The principal results of research on the radial distribution of the flux density of fast neutrons are shown in Fig. 1. The radial distributions

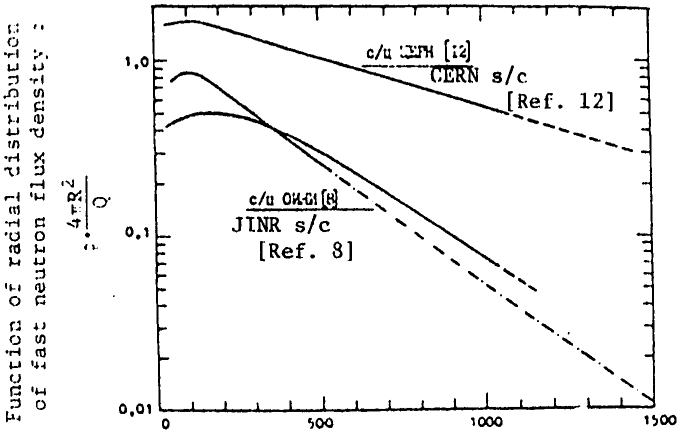

Fig. 1. Fast neutron flux densities $\phi \cdot \frac{4\pi R^2}{Q}$ at different distances from proton accelerators: Q--neutron yield into the air (neutrons per second); R--distance from the geometric center of the source (meters); ——— experimental; ----- and -·-·- approximation

are products of the neutron flux density ϕ times $4\pi R^2$ divided by the neutron yield Q from the source per unit of time [Ref. 12-14], and form a corridor of values for different accelerators. These distributions provide the best means of clarifying the difference in parameters of neutron transmission in the various media surrounding accelerator facilities. A separate curve on the same figure gives the results of measurements in the vicinity of the JINR synchrocyclotron for 660-MeV protons as determined in 1967 [Ref. 8]. Comparison of these data with measurements in the vicinity of the CERN 600-MeV synchrocyclotron as described in Ref. 12 shows that the transmission of neutrons in the medium is determined not only by the energy of accelerated protons. The effective length of attenuation of neutron fluence in the medium surrounding the

CERN synchrocyclotron [Ref. 12] was nearly three times as long as for the JINR synchrocyclotron [Ref. 8]. In this connection it becomes important to have a deeper understanding of the physical principles that determine neutron passage in the medium behind the shielding of accelerators, which will enable evaluation of the equivalent doses for personnel and the general populace with more certainty that at present both in the operation and in the planning of accelerators.

In our research an attempt is made to reach these goals by evaluating the energy distributions of neutrons and the doses at different distances from a synchrocyclotron by experimental and theoretical means.

CALCULATING THE ENERGY DISTRIBUTION OF FLUENCE AND DOSE AT GREAT DISTANCES FROM A NEUTRON SOURCE

Calculations of the field of scattered neutrons were done on the basis of a method described in Ref. 11 for two types of sources:

1) a monodirectional point source oriented perpendicular to the surface of the earth;

2) an isotropic source (in 2π steradians).

The spectrum of the neutron source was characterized as the spectrum of neutrons leaving the outer surface of a shield of ordinary concrete [Ref. 15] with the inner surface being bombarded by neutrons with maximum energy of the spectrum at 500 MeV. The spectrum assumed in the calculations is close to the neutron spectrum measured at one of the points on the outside of the synchrocyclotron shield. The water content in the concrete was taken as equal to 5% by weight. The energy distribution of the source neutrons by groups is summarized in the Table. The calculations were done without consideration of deformation of the spectrum by

TABLE

Relative contribution (%) of different energy groups of neutrons to the overall flux density

E, MeV / R, m	0.1	0.1-0.5	0.5-2	2-20	>20	Note
Behind a wall	19.5	5.3	10.7	15.0	49.5	Concrete with water content of 0.556% by weight
100	74.7	7.6	8.9	7.8	1.0	
400	62.3	9.5	11.9	12.2	4.1	
1000	58.7	11.7	14.0	10.6	5.0	
3000	39.1	9.7	13.7	19.3	18.2	

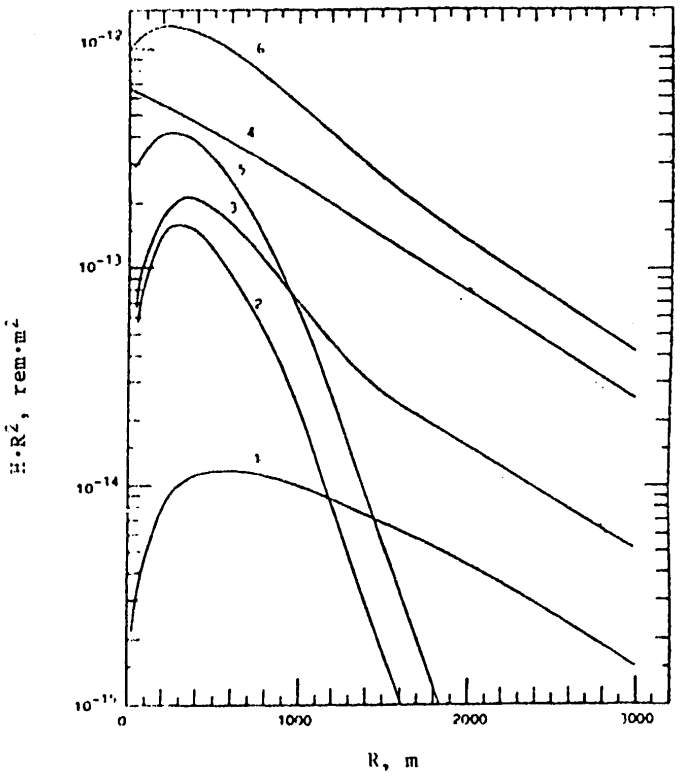

Fig. 2. Equivalent neutron dose $H \cdot R^2$ (rem·m^2) at different distances R (m) from a point source

the earth. The content of hydrogen in the air was taken as 0.1% by weight [Ref. 16]. Fig. 2 shows the calculated spatial distributions of the equivalent dose of neutrons for both types of sources. Curves 1, 2 and 3 apply to the monodirectional source; curves 4, 5 and 6 apply to the isotropic source. Curves 1 and 4 show the contribution to the equivalent dose from neutrons with energy greater than 20 MeV, curves 2 and 5 show the contribution from neutrons formed in the air as a result of scattering of source neutrons with energy of less than 20 MeV, and curves 3 and 6 show the equivalent dose from all neutrons.

The minimum neutron energy was taken as $5 \cdot 10^{-8}$ MeV, i. e. thermal neutrons were not considered in the calculations. The curves in Fig. 2 are normalized to one source neutron with energy greater than 20 MeV. On the basis of data of Ref. 11, 18, the contribution of gamma radiation to the dose equivalent was taken as negligibly small. The relative contribution of the different energy groups to the field of scattered neutrons is

given in the Table for different distances R from the monodirectional point source. The geometric idealization of the problem assumed that the calculations were being done for an infinite air medium and a source with axial symmetry. Of course the fact that the ground has a different composition and density must have an effect on the shape of the scattered neutron spectrum; however, its influence is weaker on such an integral quantity as the dose equivalent. We feel that the influence of the air-earth interface should be evaluated on the basis of available literature data, e. g. for a fission source under similar geometric conditions.

EXPERIMENT

The measurements of energy distribution and neutron dose at different distances from the synchrocyclotron were made with a Bonner spectrometer [Ref. 15], a boron-filled corona tube or an SNM helium-filled proportional counter in a cylindrical paraffin moderator with walls 120 mm thick. The measurement results are shown in Fig. 3, and are satisfactorily described by the expression

$$H{\times}R^2 = Q[h_1 \times R^2 + b(h_2 \times R^2 - h_1 \times R^2)], \qquad (1)$$

where $H{\times}R^2$ is the equivalent dose rate of neutrons at a distance of R meters from the center of the synchrocyclotron multiplied by R^2, Q is the

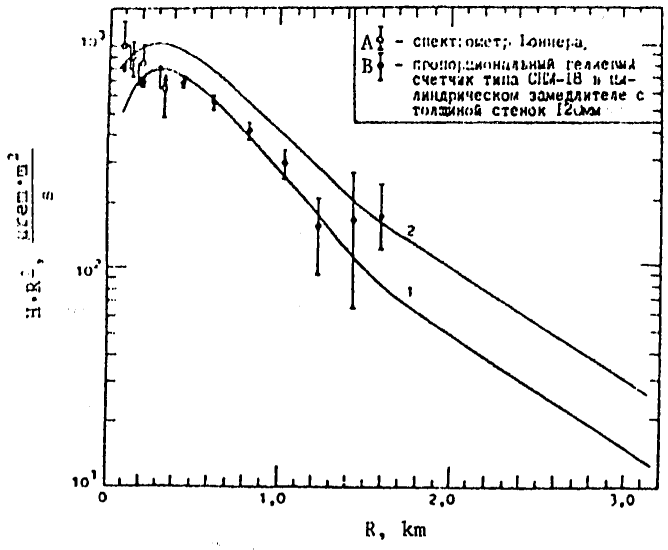

Fig. 3.
Equivalent neutron dose $H{\times}R^2$ ($\mu rem{\cdot}m^2/s$) for E < 20 MeV (1), and total equivalent dose (2) at different distances R (km) from the geometric center of a synchrocyclotron: A--Bonner spectrometer; B--SNM proportional counter in moderator with 120 mm walls

yield of neutrons with energy exceeding 20 MeV behind the shielding of the accelerator, h_1 and h_2 are the calculated equivalent dose rates of neutrons for an upwardly monodirectional point source and an isotropic emitter into a hemisphere respectively (Fig. 2), or the "responses" of the detector for different Bonner spheres, and b is a parameter that accounts for anisotropy of the source.

The parameter Q was determined in Ref. 11 on the basis of experimental data of Ref. 19, and is equal to $(1.7 \pm 0.2) \cdot 10^9$ n/s. Many years of measurements of the levels of induced radioactivity of components of the synchrocyclotron have shown that the proton current of the accelerator has increased by a factor of 1.46 ± 0.46 since 1968-1969. Thus for our calculations we assumed that

$$Q = (2.48 \pm 0.83) \cdot 10^9 \text{ n/s.}$$

Using calculated data on the "responses" of the detector in Bonner spheres (5, 10 and 12 inches) for two configurations, the experimental data of responses, and formula (1), we were able to find the mean weighted value of $b = 0.206 \pm 0.019$.

The calculated value of the total equivalent neutron dose at different distances from the synchrocyclotron [formula (1)] is shown in Fig. 3. Error does not exceed 33%.

CONCLUSIONS

Analysis of the given calculations and experimental data shows that using a simple expression like

$$HR^2 = kQ(1 - e^{-R/\mu})e^{-R/\lambda} \quad \text{[Ref. 8, 12]}$$

(see Fig. 1, curve JINR s/c) to describe the way that the equivalent neutron dose depends on distance may lead to considerable errors since the λ taken as constant in the calculations actually varies with distance and is strongly dependent on the geometry and parameters of the source at near distances (300-400 m).

A comparison of the results in Fig. 1 and Fig. 3 brings us to the conclusion that the lower envelope of the radial distribution function for fast neutron flux density apparently is valid for accelerators with "good" lateral shielding (the working model is an upwardly monodirectional point source), while the upper envelope corresponds to the model of an isotropic source emitting into 2π steradians.

In closing, the authors thank Ye. K. Gel'fand and A. Ya. Serov, who did some of the calculations for 20 MeV neutrons, and also S. P. Prusachenkov, V. N. Kulikov and P. A. Matveyev for considerable help with the measurements.

REFERENCES

1. Ye. Ye. Kovalev, "Radiatsionnyy risk na Zemle i v kosmose" [Radiation Risk on the Earth and in Space], Moscow, Atomizdat, 1976.

2. "Recommendations of the International Commission on Radiological Protection, ICRP publication 26, Pergamon Press, Oxford-New York-Frankfort, 1977.

3. S. J. Lindenbaum, ANN. REV. NUCL. SCI., No 11, 1961, p 213.

4. S. J. Lindenbaum, "Proc. Conf. on Shielding of High Energy Accelerators," New York, 1957, p 191.

5. V. N. Lebedev et al., JINR, Dubna, R-2177, 1965.

6. V. N. Lebedev, JINR, Dubna, R-2446, 1965.

7. M. M. Komochkov, V. N. Lebedev, JINR, Dubna, R-2231, 1965.

8. V. Ye. Aleynikov, V. N. Lebedev, JINR, Dubna, R9-3393, 1967.

9. L. R. Kimel' et al., JINR, Dubna, R16-6182, 1972.

10. D. N. Zaytsev et al., JINR, Dubna, R16-6185, 1972.

11. B. V. Man'ko, A. Ya. Serov, B. S. Sychev, "Trudy radiotekhnicheskogo instituta. Seriya 'Uskoriteli zaryazhennykh chastits'" [Proceedings of the Radio Engineering Institute. Series on Charged Particle Accelerators], No 14, 1973.

12. A. Rindi, R. H. Thomas, PARTICLE ACCELERATORS, No 7, 1975, p 23.

13. M. Höfert, CERN Int. report HS-RP/IR 77-19.

14. L. D. Stephens et al., Preprint LBL-3310, California, 1974.

15. B. V. Man'ko, B. S. Sychev, in: "Trudy RTI AN SSSR" [Proceedings of the Radio Engineering Institute, USSR Academy of Sciences], No 20, 1974, p 147.

16. K. P. Yakovlenko (ed.), "Kratkiy fiziko-tekhnicheskiy spravochnik" [Condensed Engineering and Physics Handbook], Moscow, Fizmatgiz, Vol 1, 1960.

17. V. Ye. Aleynikov et al., JINR, Dubna, R16-9870, 1976.

18. V. Ye. Aleynikov et al., IAEA, Vienna, VII, 1973, p 363.

19. V. Ye. Aleynikov et al., JINR, Dubna, R16-4727, 1969.

TOPICAL CATEGORIES OF PUBLICATIONS OF THE JOINT INSTITUTE FOR NUCLEAR RESEARCH

Index	Topic
1.	Experimental High-Energy Physics
2.	Theoretical High-Energy Physics
3.	Experimental Neutron Physics
4.	Theoretical Low-Energy Physics
5.	Mathematics
6.	Nuclear Spectroscopy and Radiation Chemistry
7.	Heavy Ion Physics
8.	Cryogenics
9.	Accelerators
10.	Automation of Experimental Data Processing
11.	Computer Equipment and Mathematics
12.	Chemistry
13.	Experimental Physics Techniques
14.	Investigations of Solids and Liquids by Nuclear Methods
15.	Experimental Physics of Nuclear Reactions at Low Energies
16.	Dosimetry and Physics of Shielding
17.	Theory of the Condensed State
18.	Applications of the Results and Methods of Fundamental Physical Research to Related Fields of Science and Engineering

6610
CSO: 8144/1616

VERIFYING THE CORRESPONDENCE OF RADIATION MONITORING DETECTOR READINGS TO EQUIVALENT AND ABSORBED DOSES IN THE NEUTRON BEAM OF THE IBR-30 REACTOR

Dubna PROVERKA ADEKVATNOSTI POKAZANIY DETEKTOROV DLYA DOZIMETRICHESKOGO KONTROLYA EKVIVALENTNOY I POGLOSHCHENNOY DOZAM V PUCHKE NEYTRONOV IBRa-30 in Russian, Preprint R16-12122, Joint Institute of Nuclear Research, 1979 signed to press 21 May 79 pp 1-16

[Paper by V. Ye. Aleynikov, V. A. Arkhipov, V. P. Bamblevskiy, V. V. Grechko, G. Yn. Kaskanov, M. M. Komochkov, M. I. Salatskaya and A. P. Cherevatenko, 380 copies, 16 pages]

[Text] Research was done to establish the correspondence of detector readings of personal dosimeters to the equivalent dose in a neutron beam with known energy spectrum. The paper also gives a critical evaluation of different ways of determining the equivalent neutron dose. A comparison is made of measurement results found by routine monitoring devices on the one hand, and the most reliable equivalent doses in the neutron beam on the other. Values established by a recombination dosimeter and on the basis of the measured neutron spectrum were taken as the most reliable values of the equivalent dose. The data for the two cases correspond within the error limits. The results of the work show a wide discrepancy between the readings of the investigated personal dosimeters and the equivalent dose. The low readings of film badges are due in large measure to incorrect use of the Pu-Be neutron source for graduating the badges. The method of dose determination by indium in a moderator ball, which is extensively used in practice, gives satisfactory results.

1. INTRODUCTION

In the ideal case, devices that register emissions for purposes of radiation safety should be made and graduated so as to give direct information on the maximum equivalent dose (MED) from external or internal sources

of radiation [Ref. 1]. In practice the MED is determined from the results of measurements of radiation levels and personnel monitoring. The readings of each instrument used in the measurements must be interpreted with consideration of the factors essential for the given device and dependent on the energy, time and component structure of the radiation field.

This research was undertaken to establish the extent to which the readings of various personal dosimeters correspond to the equivalent dose in a neutron beam with a known energy spectrum. A critical evaluation is also made of different methods of determining the equivalent neutron dose.

2. INSTRUMENTATION AND MEASUREMENT CONDITIONS

Table 1 shows the instruments and methods used in the measurements. Also given are the approximate ranges of energies of registered radiation, and the ranges of measured quantities. It was assumed that the most reliable values of the total equivalent dose in the beam can be obtained by a recombination dosimeter (RD). The detector of the RD was a plane-parallel three-electrode ionization chamber analogous to that described in Ref. 2 with a sensitive volume of 6 cc. The housing of the chamber was made of polymethyl methacrylate, and the electrodes were made of tissue-equivalent plastic with spacing of 2 mm. The chamber was filled with a mixture of propane (73%) and air (27%) to a total pressure of 3.5 absolute atmospheres. The total thickness of the detector was equivalent to 1 g/cm^2 of tissue.

In comparing the readings of neutron-registering detectors, we assumed that the equivalent dose calculated by using the neutron spectrum is closest to the true equivalent dose.

The instruments and detectors were irradiated in the beam of the IBR-30 reactor [Ref. 12], at distances of 8.5 and 68.5 m from the center of the core. The main measurements (including measurements with a recombination dosimeter) were made at a distance of 68.5 m. Three experiments were done. Reactor power was 15-21 kW, and pulse recurrence rate was 5 Hz. The moderator in the first experiment was a 40 mm layer of water, and in the subsequent two experiments a compound moderator was placed in the neutron beam, comprised of 30 mm of water with boron carbide and a comb-shaped water filter for enriching the beam with epithermal neutrons. The geometry of the experiment is shown in Fig. 1. The LiF detector was used to evaluate the homogeneity of the radiation field in the beam; no inhomogeneity of the field was detected within the limits of measurement error (~15%).

The information about neutron spectra was taken from Ref. 13, in which neutron spectra in the energy range of 10^{-8}-15 MeV were reconstructed by a method of statistical regularization from the readings of activation

TABLE 1

Instruments, detectors, techniques

Designation of instrument, detector, technique	Radiation	Energy range, eV	Range of measured quantity		Measurement unit
1. Recombination dosimeter (RD) [Ref. 2]	neutron gamma	unlimited $E_{\gamma} \geqslant 10^5$	$\frac{\dot{D}}{Q}$	$0.1\text{-}10^3$ 1-20	rad/hr
2. Recombination dosimeter REM-2 [Ref. 3]	neutron gamma	unlimited $E_{\gamma} \geqslant 10^5$	$\frac{\dot{D}}{Q}$	$2.5\cdot10^{-4}$-10 1-20	rad/hr
3. IFKn dosimeter [Ref. 4, 5]	neutron gamma	10^{-2}-$1.5\cdot10^7$ $E_{\gamma} \geqslant 10^4$	0.02-100 0.02-70		rem rad
4. nat.LiF powder	neutron gamma	10^{-2}-10^4 $E_{\gamma} \geqslant 2\cdot10^4$	0.5-10^2 1.0-10^3		rem r
5. TLD-600 + TLD-700 [Ref. 6]	neutron gamma	10^{-2}-10^4 $E_{\gamma} \geqslant 2\cdot10^4$	10^{-2}-10^3 10^{-2}-10^5		rem r
6. IKS-A dosimeter [Ref. 7]	gamma	$E_{\gamma} \geqslant 5\cdot10^4$	0.5-$7\cdot10^3$		rad
7. Graphite ionization chamber (KG) filled with CO_2 to 21 abs. at. [Ref. 8]	gamma	$E_{\gamma} \geqslant 10^5$	$2\cdot10^{-4}$-10^3		rad/hr
8. KID-2 dosimeter [Ref. 9]	gamma	$E_{\gamma} \geqslant 1.5\cdot10^5$	$5\cdot10^{-3}$-1.0		r
9. Indium in a moderator ball	neutron	10^{-2}-10^8	$\dot{H} \geqslant 0.075$		rem/hr
10. Activation detectors [Ref. 10, 11, 18]	neutron	10^{-2}-10^8	$\phi > 10^6$		n/cm^2·s

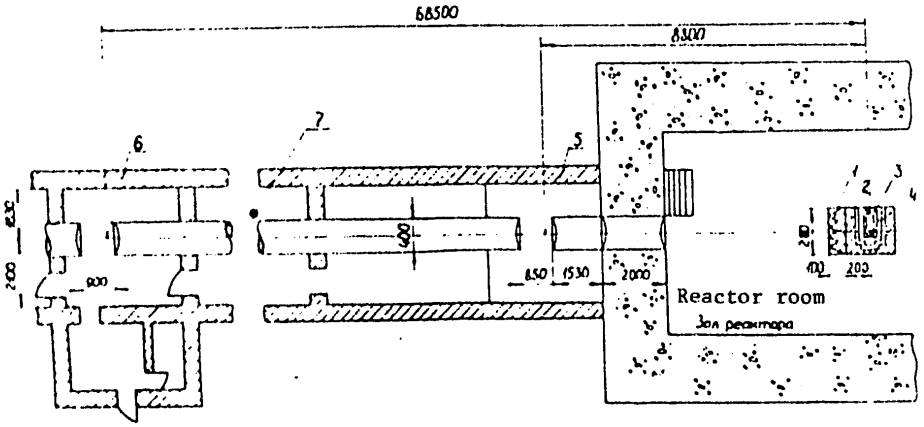

Fig. 1. Geometry of the experiment. 1--comb-shaped moderator; 2--water moderator; 3, 4--stationary and moving zones of the reactor; 5, 6--points of comparison; 7--beam monitor

neutron detectors (thermal, resonance, threshold), as well as thermal detectors in polyethylene ball moderators [Ref. 10, 11, 18] (Fig. 2, 3). For comparison, Fig. 2 gives the neutron spectrum of the IBR-30 reactor measured by a time-of-flight method [Ref. 12] at a distance of 68.6 m from the core. The values of equivalent neutron doses were determined in Ref. 13 (see Fig. 4) on the basis of the neutron spectra, using coefficients of conversion from the fluence of monoenergetic neutrons to the maximum equivalent dose [Ref. 1].

Estimates made for these spectra show that the equivalent doses calculated from the sum of the maxima and from the maximum of the sum of curves of depth distribution of radiation for monoenergetic neutrons coincide within limits of 1%.

Dose measurements by the recombination dosimeter RD were done in an elliptical phantom (35 x 24 x 20 cm), immersing the chamber into the phantom right up to its forward wall, so that the dose measured with the RD corresponds to a thickness of ~1.4 cm of phantom water. The graphite chamber was irradiated both with and without the phantom; when irradiated with the phantom, the center of the chamber was approximately 5 cm from the surface of the phantom. IDK detectors were irradiated both without a phantom, and on the surface of a phantom measuring 34 x 17 x 34 cm filled with a tissue-equivalent liquid. In measuring the dose of gamma radiation with LiF detectors and the IKS-A, shields of B_4C that attenuate the thermal neutron flux by a factor of about 10^3 were used to eliminate the effect of thermal neutrons on the detector readings.

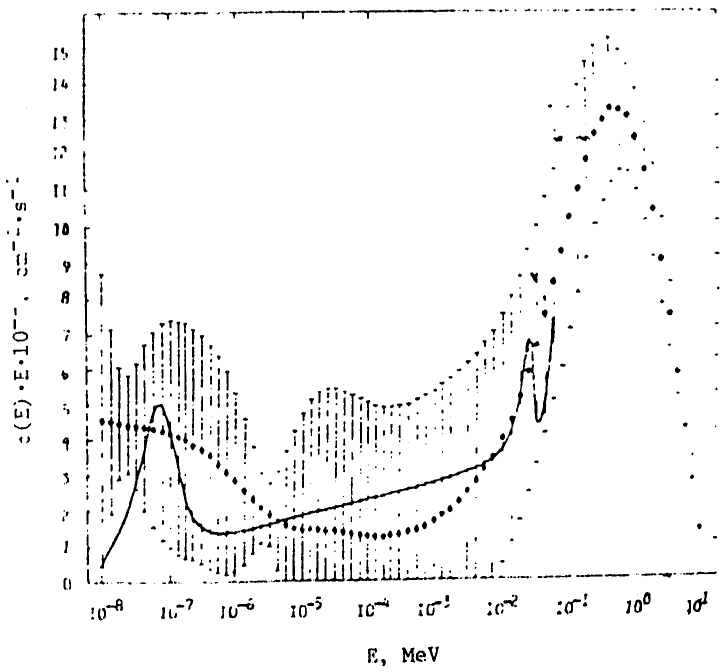

Fig. 2. Neutron spectrum $\phi(E)\cdot E$ at a distance of 68.5 m from the core of the IBR-30 reactor; $\phi(E)$ -- differential energy dependence of neutron flux density, $cm^{-2}\cdot s^{-1}\cdot MeV^{-1}$; E -- neutron energy, MeV; • -- data of Ref. 13; — -- according to data of Ref. 12

3. RESULTS

The values of the equivalent dose of neutrons measured by various detectors at a distance of 68.5 m from the center of the reactor core are shown in Table 2. The last column gives the ratios of the measured quantities to the equivalent dose calculated by using measured spectra and coefficients of conversion from the fluence of monoenergetic neutrons to the maximum equivalent dose. Table 3 gives the values of the total absorbed and equivalent dose rates of neutrons and gamma radiation, and the ratio of their doses to those measured by the recombination dosimeter RD.

Data from comparison of detector readings with irradiation at a distance of 8.8 m from the core are shown in Table 4. In the estimates of the errors in measurement of the equivalent dose rates by the indium detector in the moderator and measurement of the neutron spectrum, consideration was taken of the error in graduation (~10%) and in measurement of the radioactivities of the detectors (3-7%).

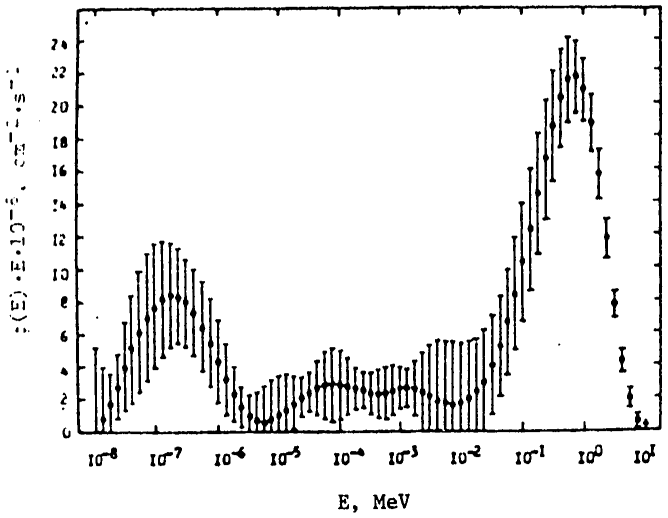

Fig. 3. Neutron spectrum $\phi(E)\cdot E$ at a distance of 8.8 m from the core of the IBR-30 reactor according to data of Ref. 13; $\phi(E)$ -- differential energy dependence of neutron flux density, $cm^{-1}\cdot s^{-1}\cdot MeV^{-1}$; E -- neutron energy, MeV

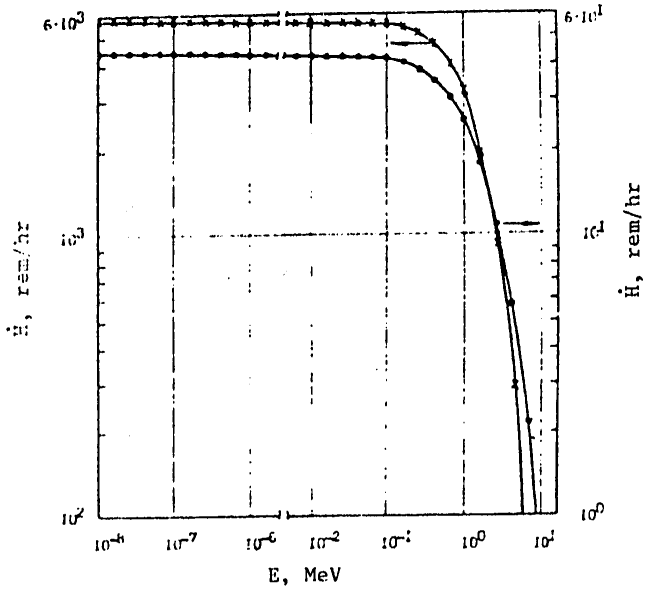

Fig. 4. Equivalent neutron dose rates $\dot{H}$ with energies greater than E according to data of Ref. 13: —×—×— at 8.8 m from the core; ···•··· at 68.5 m from the core

TABLE 2

Comparison of neutron-recording detector readings
(R = 68.5 m from the reactor core)

Designation of detectors, techniques	Equivalent dose rate $\dot{H}$, rem/hr						Ratio of detector readings to the most probable $\dot{H}$[a]
	$E_n \geq 0.5$ MeV			10^{-6} MeV $\leq E_n \leq 15$ MeV			
	1974	1975	1977	1974	1975	1977	
1. $\dot{H}$ calculated by using the neutron spectrum	--	20	33.5	--	--	14?	1.00
2. Indium in a polyethylene moderator, diam. 25.4 cm	--	--	--	57	35	57?	1.20?
3. Indium in a paraffin moderator, diam. 28 cm	--	--	--	43	34	--	1.20?
4. Recombination dosimeter RD[b]	--	--	--	(53)	(33)	(45)?	(1.12)?
5. IFKn dosimeter	(28)	(12)	(19)	(36)	(15)	(25)	(0.58) 0.58[d]
6.[c] TLD-600 + TLD-700 in IFK cassette	--	--	--	--	--	(152) 55	(3.45) 1.25
7.[c] nat.LiF powder	--	--	--	--	(18.0) 8.5	--	(0.67) 0.31

Notes: Parentheses denote the values of $\dot{H}$ (rem/hr) for exposure of a detector with phantom; a) ratio averaged over experiments for 1975 and 1977; b) readings of graphite chamber KG subtracted from the RD readings; c) readings given in r/hr; d) ratio of readings for a dose of neutrons with $E \geq 0.5$ MeV; question marks indicate illegible figures

TABLE 3

Comparison of reacings of detectors that register the total dose of gamma radiation and neutrons (R = 68.5 m from the reactor core)

Designation of detectors, techniques	Absorbed dose rate D, rad/hr			Equivalent dose rate H, rem/hr			Ratio of detector readings to RD readings a)	
	1974	1975	1977	1974	1975	1977	$\dot{D}/\dot{D}_{RD}$	$\dot{H}/\dot{H}_{RL}$
1. Recombination dosimeter (RD)	(6.0)	(4.5)	(5.6)	(54)	(34)	(46)	1.00	1.00
2. Recombination dosimeter REM-2	--	--	8.3	--	--	81	1.43	1.76
3. IFKn dosimeter	--	--	--	(39)	(16)	(27)	--	(0.59)
4. nat. LiF powder in IFK cassette (emergency dosimeter)	(24) 4.0	(26) 11	--	--	--	--	(4.89) 1.55	(0.60) b) 0.20
			--	--	--	--		
5. nat. LiF powder	(20)	(19) 11	--	--	--	--	(3.78) 2.44	(0.46) b) 0.32
			--	--	--	--		
6. TDL-600 in IFK cassette	--	--	(154) 56	--	--	--	(26.6) 9.65	(3.34) b) 1.22
7. KID-2 dosimeter	--	(2.2) 1.8	--	--	--	--	(0.49) 0.40	(0.06) b) 0.05
8. IKS-A dosimeter	(2.9) 0.74	--	--	--	--	--	(0.33) 0.12	(0.04) b) 0.01

Note: Parentheses denote the values of $\dot{H}$ (rem/hr) for exposure of detectors with phantom;
a) ratio averaged over all experiments; b) ratio of $\dot{D}$ in r/hr to $\dot{D}_{RD}$ in rem/hr

TABLE 4

Comparison of detector readings with irradiation at a distance of 8.8 m from the reactor core

Designation of detectors, techniques	Equivalent neutron dose rate, $\dot{H}_n$, rem/hr				Total dose rate $\dot{H}_n+\dot{H}_\gamma$, rem/hr[a]		Ratio of detector readings to $\dot{H}_n+\dot{H}_\gamma$ of position 1
	$E \geqslant 0.5$ MeV		10^{-8} MeV $\leqslant E_n \leqslant 15$ MeV				
	1974	1975	1974	1975	1974	1975	1975
1. $\dot{H}$ calculated by using the neutron spectrum	-	2740	-	3530	--	3590	1.00
2. Indium in a polyethylene moderator, diam. 25.4 cm	-	-	-	4270	--	4330	1.17?
3. Indium in a paraffin moderator, diam. 28 cm	-	-	4260	4100	--	4160	1.1?
4. Activation threshold detector	5600	3100	-	-	--	3160	0.88 1.13[b]
5.[c] $nat.LiF$ powder in IFK cassette (emergency dosimeter)	- -	- -	- -	- -	(2000)	(2230) 580	(0.6?) 0.1?
6.[c] $nat.LiF$ powder	-	-	-	-	(2000) 460	(1630) 450	(0.?) 0.13
7.[c] IKS-A dosimeter	-	-	-	-	(190) 79	-	-

Note: Parentheses denote values of $\dot{H}$ (rem/hr) for exposure of detectors with phantom; a) $\dot{H}_\gamma$ for positions 1-4 taken from IFK data on ORWO film; b) ratio for equivalent neutron dose with $E \geqslant 0.5$ MeV; c) readings given in r/hr; question marks indicate illegible figures

The error in determination of the equivalent dose by recombination dosimeter RD does not exceed 20%, and is due chiefly to the systematic error in determination of the quality factor [Ref. 14].

The error of the IFKn results given in the tables is ±10% (mean square error), and is due to the statistical error (~5%), the error in determining the graduation coefficient with respect to the Pu+Be source (±7%) and uncertainty of monitor readings (3-5%).

The readings of the TLD-600 and TLD-700 detectors are shown with an error of about 8% due mainly to inaccuracy in graduation. The error of results obtained with ^{nat}·LiF detectors does not exceed 20%.

Satisfactory experimental agreement (within ±15%) was observed in measurements of the dose of gamma radiation by the KG graphite chamber, X-ray ORWO film in an IFK cassette, ^{7}LiF detectors (TLD-700) and ^{nat}·LiF powder in a B_4C shield. The dose of thermal neutrons determined from readings of the TLD-600 and TLD-700 by using the sensitivity of the TLD-600 to thermal neutrons is equal to 80-84 r/rem [Ref. 15, 16], which agrees within about 15% with the dose determined from activation of gold detectors.

4. DISCUSSION OF THE RESULTS

In order to find the reasons for divergence between IFKn results and data obtained by the recombination dosimeter and spectrum, the reaction of the IFKn dosimeter was calculated on the basis of knowledge of the neutron spectrum in the beam, and the way that dosimeter sensitivity depends on incident neutron energy. Agreement within a few percent between the number of tracks found in this way and the number found in examination of emulsions under the microscope is an indication of the satisfactory quality of examination when processing individual dosimeters. However, it is incorrect in this case to uwe the graduation coefficient obtained from the Pu+Be neutron source for determining the individual equivalent dose. Calculation of the IFKn sensitivity to fast neutrons ($E \geqslant 0.5$ MeV, contributing about 75% to the equivalent neutron dose) averaged over the neutron spectrum shows that this sensitivity is about 2/3 of the value for the Pu+Be source. Because of this, plus the fact that 20% of the total neutron dose remains practically unrecorded by the IFKn dosimeter [Ref. 15], only 60% of the most probable neutron dose is recorded in the beam of the IBR-30 reactor.

The overstatement of the absorbed and equivalent dose by the REM-2 recombination dosimeter is probably due to the elevated (relative to the tissue-equivalent composition) hydrogen content in the gas filling the chamber of the REM-2.

The data given in tables 2-4 show a good outlook for using TLD detectors based on LiF in personnel monitoring on the reactor, although further

studies are needed on the readings of such detectors when they are exposed to scattered neutron fields.

The following conclusions can be drawn from analysis of the results:

1. The widely used IFKu dosimeter, when graduated by a PuBe source, understates the equivalent dose by a factor of 1.7 as compared with that found by researchers operating in fields analogous to the neutron field in the beam of the IBR-30 reactor. In this connection, graduation should be done with sources having a neutron spectrum closer to that of the reactor.

2. The numerical value of the dose in roentgens on the $^{nat.}$LiF emergency dosimeter [Ref. 17] can serve as an estimate of the equivalent dose (understates the dose by 35-40%).

3. The KID-2 dosimeter overstates the gamma radiation dose due to nuetron registration by the instrument.

4. Data found on the basis of neutron energy spectra show completely satisfactory agreement with RD data (within the limits of error).

5. The method widely used in practice of determining the equivalent dose by a thermal neutron detector (indium in the given instance) in a polyethylene ball 25.4 cm in diameter and in a paraffin ball 28 cm in diameter gives satisfactory results.

The authors thank coworkers in the radiation control group on facilities of the Neutron Physics Laboratory and the personnel monitoring group for assistance in doing the experiments and for processing the readings of the IDK detectors.

REFERENCES

1. "ICRU Rep. 20: Radiation Protection, Instrumentation and its Application," International Commission on Radiation Units and Measurements, Washington, D. C., 1971, p 7.

See also: "Radiatsionnaya bezopasnost'. Velichiny, edinitsy, metody i pribory. Doklady XIX i XX MKRE" [Radiation Safety. Quantities, Units, Methods and Instruments. ICRU Reports 19 and 20], translation from English, edited by L. B. Kerim-Markus, Atomizdat, Moscow, 1974.

2. M. Zel'chinskiy et al., Joint Institute of Nuclear Research [JINR], R16-5383, Dubna, 1970.

3. M. Zelczyinski, K. Zarnowiecki, "A Differential Recombination Chamber" in "Neutron Monitoring," IAEA, Vienna, 1966, p 125.

4. L. S. Zolin, V. N. Lebedev, M. I. Salatskaya, ATOMNAYA ENERGIYA, Vol 13, 1962, p 467.

5. M. M. Komochkov, M. I. Salatskaya, JINR, R16-9780, Dubna, 1976.

6. K. Becker, "Solid-State Dosimetry," CRC Press, Cleveland Ohio, 1973.

7. I. A. Bochvar et al., "Metod dozimetrii IKS" [The IKS Method of Dosimetry], Moscow, Atomizdat, 1977.

8. M. Zielczynski, "Report IBJ Nr 148/XIX/D/B, Warsaw, 1973, p 8.

9. V. I. Skotnikov, V. V. Lapkin, "Ekspluatatsiya i remont apparatury dlya izmereniya ioniziruyushchikh izlucheniy. Vyp. 3. Dozimetry" [Operation and Repair of Equipment for Measuring Ionizing Radiation. No 3. Dosimeters], edited by Ye. A. Levandovskiy, Moscow, Atomizdat, 1973, p 8.

10. V. Ye. Aleynikov et al., JINR, R16-9123, Dubna, 1975.

11. V. I. Aleynikov et al., JINR, R16-9621, Dubna, 1976.

12. V. V. Golikov et al., JINR, 3-5736, Dubna, 1971.

13. V. P. Bamblevskiy, V. V. Grechko, JINR, B1-16-12123, Dubna, 1979.

14. M. Zel'chinskiy, "Determining Radiation Quality by Recombination Methods," in "Biophysical Aspects of Radiation Quality," Second Panel Report, IAEA, Vienna, 1968, p 125.

15. J. R. Harvey et al., "Personal Dosimeter for Measuring the Dose from Thermal and Intermediate-Energy Neutrons and from Gamma and Beta Radiations" in "Proceedings of the Symposium on Neutron Monitoring for Radiation Protection Purposes," Vol 2, IAEA, Vienna, 1973, p 199.

16. S. Tanaka, J. Furuta, J. NUCL. INSTR. AND METH., No 133, 1976, p 495.

17. M. M. Komochkov, M. I. Salatskaya, JINR, R16-8175, Dubna, 1974.

18. V. P. Bamblevskiy, V. V. Grechko, JINR, R16-12069, Dubna, 1978.

6610
CSO: 8144/1614

UDC 539.1 (076.1)

LABORATORY MANUAL ON NUCLEAR PHYSICS

Moscow SBORNIK LABORATORNYKH RABOT PO YADERNOY FIZIKE in Russian 1979 signed to press 3 Apr 79 pp 2-5

[Annotation and Table of Contents from laboratory manual edited by professor K. N. Mukhin. Second edition. Moscow, Atomizdat, 1979, 5800 copies, 272 pages]

[Text] This book considers problems in the areas of radioactivity, nuclear spectroscopy, neutron physics, the physics of elementary particles, the physics of cosmic rays, the methods of the applications of nuclear physics etc. The proposed laboratory manual (the first edition was printed in 1970) makes it possible for students to obtain the necessary complex of practical knowledge and work habits with modern equipment and modern research methods in the area of nuclear physics. The manual includes new in principle material (work with on-line computers, computer processing of measurement data, the use of modern electronics in nuclear physics experiments).

The manual is intended for upperclassmen in physio-technical and engineering-physics institutes specializing in the area of nuclear and applied physics, as well as students in VUZ and VTUZ [Higher technical educational institution] in which a course on nuclear physics is given.

29 tables; 108 figures; bibliography contains 41 items.

Table of Contents

[158-2291]

2291
CSO: 1862

UDC 621.039

NUCLEAR TECHNOLOGY

Moscow YADERNAYA TEKHNOLOGIYA in Russian 1979 signed to press 27 Jul 79 pp 2, 334-336

[Annotation and Table of Contents from textbook for VUZ by V. P. Shvedov, V. M. Sedov, I. L. Rybal'chenko and I. N. Vlasov, Moscow Atomizdat 3850 copies, 336 pages]

[Text] The basis of this textbook are lecture courses given for several years at the Eningeering Physio-Chemical Department of the Leningrad Technological Institute imeni Lensovet.

The book discusses practically all problems related to the technology of producing and reprocessing nuclear fuel. Designs of nuclear reactors and problems of their operation are considered, as well as the problem of rendering radioactive wastes harmless. Principles of designing plants, technological equipment and laboratories for radio nuclides are discussed. Serious attention is devoted to the deactivation of buildings and equipment of radio-chemical production facilities and the preservation of the environment.

The textbook is intended for students of technological and polytechnical VUZ and universities specializing in the radio-chemical processes of nuclear power and radio-chemistry; it may also be useful to specialists involved in water purification technology and rendering radioactive wastes harmless, the deactivation of equipment and protection of the environment.

107 pictures, bibliography contains 56 items.

Table of Contents

2291
CSO: 1862

OPTICS AND SPECTROSCOPY

UDC 621.314.26

FOUR PHOTON PARAMETRIC RESONANCE UPCONVERSION OF AN INFRARED SIGNAL FREQUENCY IN A BROAD BAND PUMPING FIELD

Moscow KVANTOVAYA ELEKTRONIKA in Russian Vol 7, No 6, Jun 80 pp 1348-1349 manuscript received 8 Jan 80

[Article by N.A. Iskanderov, V.A. Kudryashov and I.N. Matveyev]

[Text] The process of parametric upconversion of an IR signal frequency for the case of two-photon pumping resonance, the spectral width of which significantly exceeds the characteristic widths of the lines of the atomic transitions, is analyzed theoretically. It is shown that the maximum steady-state conversion efficiency in a broad band field differs only to a minor extent from the maximum conversion efficiency in a regular and monochromatic field. A dynamic gain in the IR signal conversion efficiency is possible in the nonsteady-state interaction mode.

Four-photon parametric resonance upconversion of a frequency in regular and monochromatic fields has been studied rather completely and in detail [1, 2]. However, in the experimental realization of this process, the pumping spectral width was significantly greater than the characteristic width of the atomic transition lines [3, 4].

The process of four-photon upconversion of an IR signal frequency is treated theoretically in this paper for the case of two-photon resonance of a specified pump field. The problem is solved taking into account the relaxation processes which occur when the field is turned on, the complex amplitude of which is steady-state and gaussian, while the frequency spectrum is lorentzian or gaussian with a width of $\Delta\omega \gg T_{1,2}^{-1}$ ($T_{1,2}$ are the relaxation times for a two-level system).

In approximating the specified pump field and IR signal, the system of equations which describes the frequency conversion process under consideration, has the form [2]:

$$\begin{aligned} T_1\dot{n}+n-n_0 &= p^*A_1^2+pA_1^{*2},\\ T_2\dot{p}+(1+i\delta T_2)p &= -{}^1/_2\,A_1^2 n,\\ \frac{\partial A_3}{\partial z} &= \gamma_3 pA_2. \end{aligned} \tag{1}$$

Here, n is the difference in the populations of the lower and upper levels; p is the polarization; the function $A_l=\sqrt{2q\sqrt{T_1T_2}}\,\mathcal{E}_l$ is proportional to the complex amplitude $\mathcal{E}_l$ (l = 1 for pumping, 2 for an infrared signal and 3 for the converted radiation) of the field $E_l(t)$ = = $=\mathcal{E}_l(t)e^{-i\omega_l t}+\text{comp.conj.}(t\geqslant 0)$; $E_l(t<0)=0$; $\gamma_3=\gamma_4(T_2/T_1)^{1/2}$; $\delta=\omega_{12}-2\omega+\Omega_1+\Omega_2$.

and the remaining symbols are the same as in [2].

The normalized average IR signal conversion efficiency is $\bar{\eta}=\overline{4pp^*}$. We shall assume that the pump spectrum width, $\Delta\omega$, excited by the two-photon transition, satisfies the relationship $\Delta\omega T_{1,2} \gg 1$. This condition makes it possible to consider $A^2(t)$ as complex white noise, for which:

$$\langle A^2(t)A^{*2}(t+\tau)\rangle = C\delta(\tau), \tag{2}$$

where the correlation constant is $C = 4I_1^2/\Delta\omega$ for a lorentz spectrum and $C = (\pi/2)4I_1^2/\Delta\omega$ for a gaussian spectrum. I_1 is the integral pumping field intensity.

By employing the averaging procedure given in [5], we derive the following system of equations for the determination of the timewise evolution of $\overline{pp^*}$ taking (2) into account:

$$\begin{aligned} &\dot{\bar{n}}+\alpha_1(1+{}^1/_2\alpha_2 C)\bar{n}=\alpha_1 n_0,\\ &\dot{\bar{n}}^2+2\alpha_1(1+{}^1/_2\alpha_2 C)\bar{n}^2=2\alpha_1^2 C\overline{pp^*}+2\alpha_1 n_0\bar{n},\\ &\dot{\overline{pp^*}}+2\alpha_2(1+{}^1/_4\alpha_1 C)\overline{pp^*}={}^1/_4\alpha_2^2 C\bar{n}^2, \end{aligned} \tag{3}$$

where $\alpha_1 = 1/T_1$ and $\alpha_2 = 1/T_2$.

In the steady-state conversion mode, where the time derivatives in (3) can be disregarded, we find for the normalized average conversion efficiency:

$$\bar{\eta} = \frac{y}{(1+y)[1+(1+\alpha_1/2\alpha_2)y]}, \tag{4}$$

where $y = \alpha_2 C/2$.

When

$$y = 1/\sqrt{1+\alpha_1/2\alpha_2} \tag{5}$$

the conversion efficiency of (4) has a maximum value of:

$$\bar{\eta}_{max} = 1/(1+\sqrt{1+\alpha_1/2\alpha_2})^2,$$

which differs only slightly from the maximum conversion efficiency in a regular and monochromatic field. Since C depends both on I_1 and on $\Delta\omega$, then condition (5) can be treated in two ways: as determining either the optimum intensity for a specified $\Delta\omega$, or the optimum spectral width for a specified I_1. It should be noted that the calculation of the optimum intensity from formula (5) and the average conversion efficiency from formula (4) is correct only for the condition where $\Delta\omega T_{1,2} >> 1$.

The average IR signal conversion efficiency $\bar{\eta}$ is shown in Figure 1 as a function of the correlation constant C. It should be kept in mind that for the same values of I_1 and $\Delta\omega$, the correlation constant depends on the form of the frequency spectrum, and in particular, where $\alpha_2 C/2 << 1$, when the two-photon transition saturation effect is not manifest, the parametric frequency conversion in a pumping field with a gaussian frequency spectrum is $(\pi/2)^{1/2}$ more efficient than in a field with a lorentz frequency spectrum.

The numerical solution of (3) on a computer shows that in the steady-state conversion mode, it is possible to have a dynamic gain in the conversion efficiency, something which is also illustrated in Figure 2.

The results of this paper are generalized without difficulty to the case of (k + 2)-photon resonance parametric upconversion of an IR signal frequency for the case of k-photon resonance of a specified broad band pump field, by the following substitution of the form of the correlation constants: $C = 4(k-1)!I_1^k/\Delta\omega$ for a lorentz spectrum and $C = 2k!I_1^k/\Delta\omega\sqrt{k/\pi}$ for a gaussian spectrum.

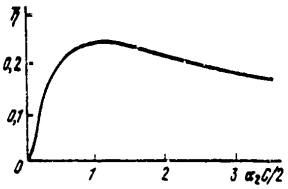

Figure 1. The steady-state conversion efficiency as a function of the correlation constant ($T_2 = 0.1T_1$).

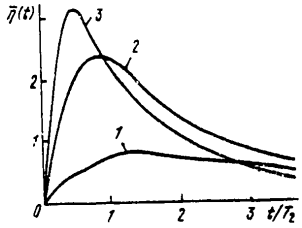

Figure 2. The timewise evolution of the conversion efficiency ($T_2 = 0.1T_1$) when $\alpha_2 C/2 = 1$ (1), 5 (2) and 10 (3).

The authors are deeply grateful to Yu.Ye. D'yakov for the useful discussions.

BIBLIOGRAPHY

1. V.S. Butylkin, A.Ye. Kaplan, Yu.G. Khronopulo, Ye.I. Yakubovich, "Rezonansnyye vzaimodeystviya sveta s veshchestvom" ["Resonance Interactions of Light with Matter"], Moscow, Nauka, 1977.

2. V.I. Anikin, K.N. Drabovich, A.D. Dubovik, ZHETF [JOURNAL OF EXPERIMENTAL AND THEORETICAL PHYSICS], 72, 1,727, (1977).

3. D.M. Bloom, J.T. Yardley, J.F. Young, S.E. Harris, APPL. PHYS. LETTS., 24, 427, (1974).

4. E.A. Stappaerts, S.E. Harris, J.F. Young, APPL. PHYS. LETTS., 29, 669, (1976).

5. Yu.Ye. D'yakov, KRATKIYE SOOBSHCHENIYA PO FIZIKE, FIAN [BRIEF COMMUNICATIONS ON PHYSICS OF THE USSR ACADEMY OF SCIENCES INSTITUTE OF PHYSICS IMENI P.N. LEBEDEV], No 7, 49, (1971).

8225
CSO: 1862

UDC 621.373.038.84

THE RADIATIVE CHARACTERISTICS OF A QUARTZ CONTAINED PLASMA DYNAMIC DISCHARGE IN THE 200 TO 250 NANOMETER RANGE

Moscow KVANTOVAYA ELEKTRONIKA in Russian Vol 7, No 6, Jun 80 pp 1340-1342 manuscript received 9 Dec 79

[Article by G.N. Kashnikov, V.K. Orlov, A.N. Panin, A.K. Piskunov and V.A. Reznikov]

[Text] The characteristics of radiation in a range of 200 to 250 nm from the region of shock interaction of plasma flows produced in a quartz tube by two magnetoplasma compressors are studied. With a pulse width of a few microseconds, a radiation brightness temperature of 27,000° is achieved at a wavelength of 205 nm.

It was demonstrated in the literature [1, 2] that with the passage of high power ultraviolet radiation, reversible opaqueness of quartz is observed in a spectral range of $\lambda < 300$ nm. The studies were carried out with relatively long electrical discharge pulses (30 to 300 μsec). The reversible opaqueness was explained by the vaporization of a fine layer of quartz heated by the UV radiation up to 3,000-4,000° and the absorption of the radiation by the quartz vapors. Gas protection of the quartz surface was studied in paper [2] using CO molecules as a filter, where these are formed during the vaporization of polyformaldehyde exposed to the radiation. A radiation brightness temperature of 19,000° was achieved in the 200 nm range. A portion of the discharge radiation in such a design is lost in the lattice of the polyformaldehyde placed inside the quartz source.

It is of interest to study the transmission of short wave UV radiation through a quartz wall under conditions of high power short electrical discharge because of the fact that the mechanism for reversible opaqueness should have inertia.

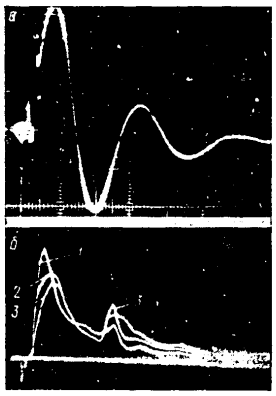

Figure 1. The current pulses of the MPK's [magnetoplasma compressors] (a) and the radiation at λ = = 205 nm (b) of the shock interaction region of the plasma dynamic dishcarge where E_{el} = = 2.5 (1), 2 (2) and 1.4 KJ (3) (the horizontal sweep is 5 μsec/division).

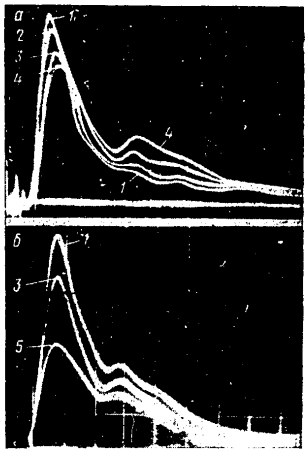

Figure 2. Radiation pulses at λ = = 220 (a) and 250 nm (b) of the plasma dynamic discharge for E_{el} = 2.5 (1), 2.2 (2), 2.0 (3), 1.7 (4) and 1.3 KJ (5) (the horizontal sweep is 5 μsec/ /division).

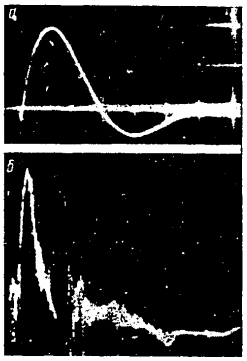

Figure 3. The MPK current pulses (a) and the radiation at λ = 205 nm (b) of the plasma dynamic discharge where E_{el} = 5.8 KJ (the horizontal sweep is 10 μsec/division).

The studies were performed with a quartz source in the region of shock interaction of plasma flows produced by two magnetoplasma compressors (MPK) of the erosion type, operating into each other. The configuration of the experiment is similar to that given in paper [3] and consists of two MPK's, placed at the end faces of a quartz tube made of KU-2, 280 mm long with an internal diameter of 40 mm. The volume of the source was pumped out down to $2 \cdot 10^{-2}$ mm Hg through annular gaps between the external electrodes of the MPK's and the quartz tube. Power was supplied to each MPK from a capacitor with the following parameters: C = 80 microfarads, U = 8 KV and L = 20 nanohenries. The width of a half period of the current pulse of the resonant circuit was T/2 = 7 μsec, the attenuation was $R/2L = 6 \cdot 10^4$ sec^{-1} and $dI/dt = 8.3 \cdot 10^{10}$ a/sec. The energy delivered to the plasma was 0.5 times the energy stored in the capacitors. The discharge was initiated by feeding a high voltage low power pulse (0.1 J, 2 μsec) to an additional electrode installed on the external electrode of each MPK. The radiation brightness temperature was measured with an ISP-30 spectrograph operating as a monochromator, and a F-7 photodetector, installed at the output of the spectrograph. The circuit was calibrated using an EV-45 reference calibration source.

A dense plasma formation about 14 cm long arises in the region of shock interaction in the quartz tube. Oscilloscope traces of the radiation pulses of the shock interaction region in a wavelength range of 205 nm with a spectral width of 3 nm are shown in Figure 1b, while oscilloscope traces of the radiation pulses in a wavelength range of 220 nm with a spectral width of 6 nm are shown in Figure 2a. The delay of the light pulse with respect to the discharge pulse was 3 μsec, which corresponds to an initial propagation velocity of the plasma flows of about 50 km/sec.

With an energy input into the plasma of E_{el} = 2.5 KJ, the maximum radiation power is achieved in the second to third microsecond, after which there follows a falling off, which is due to the vaporization of the wall of the quartz tube and the blocking of the discharge radiation. The maximum brightness temperature T_b of the λ = 205 nm radiation amounts to 27,000°. The waveform of the radiation pulse of the plasma in front of the quartz wall can be estimated from oscilloscope traces of the radiation at λ = 250 nm (Figure 2b), for which there is no significant absorption by the quartz, something which is confirmed by the linear dependence of the radiation energy on the energy input into the discharge. The radiation pulse width at a wavelength of λ = 205 nm (E_{el} = 2.5 KJ) is cut in half at the half-height value as compared to the similar parameter for radiation at λ = 250 nm, while the maximum is shifted towards the onset of the discharge With a reduction in the energy input, the reversible opaqueness effect is less pronounced, something which leads to a widening of the first peak and a rise in the amplitude of the second radiation peak, corresponding to the second half-period of the current pulse (see Figure 1). With a change in the energy input into the discharge, the radiation power distribution at λ = 205 and 220 nm in the second peak is the inverse of the distribution in the first peak. The losses due to absorption by the quartz increase by the 13th microsecond by a factor of three to four with an increase in E_{el} from 1.5 up to 2.5 KJ. Keeping in mind that the rate of vaporization of the quartz is equal to 10 to 20 cm/sec [1], the absorption factor K of the quartz in the 13th microsecond amounts to 10^4 cm^{-1}, a figure which is approximately an order of magnitude higher than the measured values of K in the indicated literature for λ = 250 nm.

An oscilloscope trace of the radiation pulse at λ = 205 nm of the shock interaction region of MPK plasma flows powered by electrical pulses with a width of T/2 = 26 μsec and a total energy in the plasma of 5.8 KJ is shown for comparison in Figure 3. The maximum radiation brightness temperature is T_b = 22,000°, while the bulk of the radiation energy is lost due to reversible opaqueness of the quartz.

Thus, the quartz of the source, based on a plasma dynamic discharge, can pass radiation pulses with $\lambda \approx$ 200 nm and T_b = 27,000° having a width of a few microseconds without significant losses because of the inertia of the mechanism of reversible opaqueness of the quartz. A further rise in the radiation brightness temperature is possible in the spectral range considered here with an increase in the rate of energy input into the discharge by the MPK's and the use of more difficultly fusible optical material instead of quartz (for example, leukosapphire). This type of optical source can find applications in pumping photodissociation lasers in the visible and ultraviolet band using vapors of I_2 [4], XeF_2 [5] and $HgBr_2$ [6].

BIBLIOGRAPHY

1. N.N. Ogurtsova, I.V. Podmoshenskiy, V.M. Shelemina, TEPLOFIZIKA VYSOKIKH TEMPERATUR, 16, 744, (1978).

2. Ye.M. Golubev, N.N. Ogurtsova, I.V. Podmoshenskiy, P.N. Rogovtsev, ZHPS [JOURNAL OF APPLIED SPECTROSCOPY], 20, 577, (1974).

3. A.S. Kamrukov, G.N. Kashnikov, N.P. Koslov, V.K. Orlov, Yu.S. Protasov, PIS'MA V ZHTF [LETTERS TO THE JOURNAL OF TECHNICAL PHYSICS], 3, 1,331, (1977).

4. N.G. Basov, I.S. Datskevich, V.S. Zuyev, L.D. Mikheyev, A.V. Startsev, A.P. Shirokikh, KVANTOVAYA ELEKTRONIKA, 4, 638, (1977).

5. N.G. Basov, V.S. Zuyev, L.D. Mikheyev, D.B. Stavrovskiy, V.I. Yalovoy, KVANTOVAYA ELEKTRONIKA, 4, 2,453, (1977).

6. S.P. Bazhulin, N.G. Basov, V.S. Zuyev, Yu.S. Leonov, Yu.Yu. Stoylov, KVANTOVAYA ELEKTRONIKA, 5, 684, (1978).

[173-8225]

8225
CSO: 1862

END